

1 **Hydrological (in)stability in southern Siberia during the Younger Dryas and**  
2 **Early Holocene**

3  
4 **P. Harding** <sup>a,b\*</sup>, E. V. Bezrukova <sup>c,d</sup>, S. S. Kostrova <sup>c, e</sup>, J. H. Lacey <sup>f</sup>, M. J. Leng <sup>f,g</sup>,  
5 H. Meyer <sup>e</sup>, L. A. Pavlova <sup>c</sup>, A. Shchetnikov <sup>h, i, j</sup>, M. V. Shtenberg <sup>k</sup>, P. E. Tarasov <sup>l</sup>,  
6 A.W. Mackay <sup>a</sup>.

7  
8 *a. Environmental Change Research Centre, Department of Geography, University*  
9 *College London, London, WC1E 6BT, UK.*

10 *b. Centre for Quaternary Research, Dept. of Geography, Royal Holloway, TW20 0EX,*  
11 *UK.*

12 *c. Vinogradov Institute of Geochemistry, SB RAS, Irkutsk, 664033, Russia.*

13 *d. Irkutsk Scientific Center, SB RAS, Irkutsk, 664033, Russia.*

14 *e. Alfred Wegener Institute, Helmholtz Centre for Polar and Marine Research,*  
15 *Research Unit Potsdam, Potsdam, 14473, Germany.*

16 *f. National Environmental Isotope Facility, British Geological Survey, Keyworth,*  
17 *NG12 5GG, UK.*

18 *g. Centre for Environmental Geochemistry, School of Biosciences, University of*  
19 *Nottingham, LE12 5RD, UK.*

20 *h. Institute of the Earth's Crust, SB RAS, Irkutsk, 664033, Russia.*

21 *i. Irkutsk State University, 2 Chkalov St., Irkutsk, 664003, Russia.*

22 *j. Geological Institute, Russian Academy of Sciences, Pyzhevsky lane 7, 119017,*  
23 *Moscow, Russia.*

24 *k. Institute of Mineralogy, UB RAS, Miass, 456317, Russia.*

25 *I. Institute of Geological Sciences, Palaeontology, Freie Universitaet Berlin, Berlin,*  
26 *12249, Germany.*

27 **\*Corresponding author: poppy.harding@rhul.ac.uk**

28

29 **Abstract:**

30 Southern Siberia is currently undergoing rapid warming, inducing changes in  
31 vegetation, loss of permafrost, and impacts on the hydrodynamics of lakes and rivers.  
32 Lake sediments are key archives of environmental change and contain a record of  
33 ecosystem variability, as well as providing proxy indicators of wider environmental and  
34 climatic change. Investigating how hydrological systems have responded to past shifts  
35 in climate can provide essential context for better understanding future ecosystem  
36 changes in Siberia. Oxygen isotope ratios within lacustrine records provide  
37 fundamental information on past variability in hydrological systems. Here we present  
38 a new oxygen isotope record from diatom silica ( $\delta^{18}\text{O}_{\text{diatom}}$ ) at Lake Baunt ( $55^{\circ}11'15''\text{N}$ ,  
39  $113^{\circ}01,45''\text{E}$ ), in the southern part of eastern Siberia, and consider how the site has  
40 responded to climate changes between the Younger Dryas and Early to Mid Holocene  
41 (ca. 12.4 to 6.2 ka cal BP). Excursions in  $\delta^{18}\text{O}_{\text{diatom}}$  are influenced by air temperature  
42 and the seasonality, quantity, and source of atmospheric precipitation. These variables  
43 are a function of the strength of the Siberian High, which controls temperature, the  
44 proportion and quantity of winter versus summer precipitation, and the relative  
45 dominance of Atlantic versus Pacific air masses. A regional comparison with other  
46 Siberian  $\delta^{18}\text{O}_{\text{diatom}}$  records, from lakes Baikal and Kotokel, suggests that  $\delta^{18}\text{O}_{\text{diatom}}$   
47 variations in southern Siberia reflect increased continentality during the Younger  
48 Dryas, delayed Early Holocene warming in the region, and substantial climate  
49 instability between  $\sim 10.5$  to  $\sim 8.2$  ka cal BP. Unstable conditions during the Early  
50 Holocene thermal optimum most likely reflect localised changes from glacial melting.  
51 Taking the profiles from three very different lakes together, highlight the influence of  
52 site specific factors on the individual records, and how one site is not indicative of the

53 region as a whole. Overall, the study documents how sensitive this important region  
54 is to both internal and external forcing.

55 **Keywords:** LGIT, Siberia, Paleoclimate, Paleohydrology, Stable-isotopes, diatoms.

## 56 **1. Introduction:**

57 Anthropogenic climate change is having a significant impact on hydrology and  
58 ecosystems globally. Reconstructing past palaeohydrological responses to climate  
59 change is fundamental for assessing potential future responses to climate change  
60 (Swann et al., 2018). Southern Siberia is currently undergoing climate warming at a  
61 rate considerably higher than the global average (Tingley and Huybers, 2013). The  
62 effects of this are significant, especially the reduction in hemiboreal forests (Deluca  
63 and Boisvenue, 2012) through changes to wildfire frequency (Tchebakova et al.,  
64 2011), increased melting of permafrost (Romanovsky et al., 2010), and changes to  
65 seasonally-ice covered lacustrine ecosystems (Moore et al., 2009; Tchebakova et al.,  
66 2009; Tchebakova et al., 2011). In some regions, the drivers of past climatic events  
67 have been well studied (Bond, 1997; Bond et al., 2001; Hoek and Bos, 2007; Teller et  
68 al., 2002; Wanner et al., 2011), and their impacts on hydrology and ecosystems are  
69 well defined (Brauer et al., 2008; Fletcher et al., 2010; Lane et al., 2013; Rach et al.,  
70 2014). However, other critical regions, such as continental ecotones, are relatively  
71 understudied. For example, the majority of studies in southern Siberia are focussed  
72 on the Lake Baikal ecosystem (Katsuta et al., 2018; Mackay et al., 2013a, 2011, 2005;  
73 Morley et al., 2005; Prokopenko et al., 2002, 1999; Prokopenko and Williams, 2004;  
74 Rioual and Mackay, 2005; Swann et al., 2018; Tarasov et al., 2007; Williams et al.,  
75 1997). Further research is, thus, essential to investigate hydrological changes outside  
76 of Lake Baikal's immediate catchment.

77 Globally, the transition to the current interglacial sees a number of important climatic  
78 events, with Younger Dryas cooling marking the last stage of the glacial from ~13 ka  
79 cal BP, and rapid Holocene warming from ~11.7 ka cal BP (Blockley et al., 2012;  
80 Rasmussen et al., 2014), both influencing atmospheric regimes (Steffensen et al.,

81 2008; Wang et al., 2001). The Early Holocene also features abrupt climatic events at  
82 ~11.4, 11.1, 9.3 and 8.2 ka cal BP (Blockley et al., 2018; Dykoski et al., 2005; Heiri et  
83 al., 2004; Hoek and Bos, 2007; Rasmussen et al., 2014; Zhang et al., 2018), thought  
84 to be linked to freshwater outbursts, reducing thermohaline circulation (THC) in the  
85 North Atlantic (Barber et al., 1999; Rohling and Pälike, 2005; Teller et al., 2002), solar  
86 minima (Bond et al., 2001; Dykoski et al., 2005), and volcanic eruptions (Anchukaitis  
87 et al., 2010; Cole-Dai et al., 2013; Sigl et al., 2015). This period provides important  
88 context for future climate changes, as much of the temperature variability is within the  
89 range predicted for the next 100-200 years (2-4°C) (Collins et al., 2013). Moreover,  
90 destabilisation of ice sheets, THC variability and changing solar activity are also  
91 important elements of future climate scenarios (Collins et al., 2013).

92 The Younger Dryas is documented across the Northern Hemisphere (Brauer et al.,  
93 2008; Brooks et al., 2012; Coope et al., 1998; Heiri and Millet, 2005), with cooling  
94 thought to be driven by changes in Atlantic meridional overturning circulation (Lane et  
95 al., 2013), which are then propagated to the atmosphere (Bakke et al., 2009). The  
96 Transbaikal region of southern Siberia experienced strong seasonality during the  
97 Younger Dryas due to high obliquity, inducing cold winters (Bush, 2005). High K<sup>+</sup>  
98 concentrations in the GISP2 ice core during the latter stages of the Younger Dryas  
99 suggest that a strong Siberian High dominated winter climates (Mayewski et al., 2004)  
100 (Tarasov et al., 2009). A strong Siberian High drives a stronger East Asian Winter  
101 Monsoon, through a larger pressure gradient between the Siberian High and Aleutian  
102 Low (Tubi and Dayan, 2013), resulting in weaker East Asian Summer Monsoons. The  
103 latter is reflected in higher isotope values from Chinese speleothems in Hulu (Wang  
104 et al., 2001), Dongge (Dykoski et al., 2005) and Sanbao (Dong et al., 2010) caves,  
105 and cold reconstructed temperatures in Lake Suigetsu, Japan (Schlölaut et al., 2017).

106 During the Early Holocene, maximum summer insolation values occurred (Bush,  
107 2005), leading to the Holocene Thermal Maximum at ~10.0 and 6.0 ka cal BP (Liu et  
108 al., 2014). At higher latitudes, particularly away from large ice sheets, a shorter thermal  
109 maximum occurred between ~10.0 and 8.0 ka cal BP (Jansen et al., 2007; Renssen  
110 et al., 2012), coupled with strong seasonality (Biskaborn et al., 2016; Bush, 2005).

111 The isotopes of diatom silica are widely recognised as proxies for environmental  
112 change, such as the use of the oxygen isotope ratios to reconstruct palaeohydrology  
113 (Leng and Barker, 2006; van Hardenbroek et al., 2018).  $\delta^{18}\text{O}$  is influenced by changes  
114 in external environmental and climatic factors, including the quantity or source of  
115 precipitation, atmospheric temperature variability, and evaporation regimes.  $\delta^{18}\text{O}_{\text{diatom}}$   
116 reconstructions are available for key southern Siberian sites, including Lake Baikal  
117 (Mackay et al., 2013b, 2011) and Lake Kotokel, located to the east of the Baikal central  
118 basin (Kostrova et al., 2013b, 2014, 2016). In Lake Baikal,  $\delta^{18}\text{O}_{\text{diatom}}$  variability has  
119 been linked to factors including the relative proportion of southern versus northern  
120 rivers feeding the lake, due its enormous catchment (Mackay et al., 2011), and at Lake  
121 Kotokel to the interplay of evaporation and the  $\delta^{18}\text{O}$  of precipitation, which is linked to  
122 air temperature and atmospheric circulation (Kostrova et al., 2013b, 2014, 2016).

123 This study aims to increase the understanding of palaeohydrological changes that  
124 have occurred at the sensitive discontinuous-continuous permafrost boundary in  
125 Siberia. We present new  $\delta^{18}\text{O}_{\text{diatom}}$  data from a sediment core from Lake Baunt  
126 (below), one of the first analyses of lake records with a localised catchment spanning  
127 the Younger Dryas to Mid Holocene in the northern regions of southern Siberia. We  
128 combine our  $\delta^{18}\text{O}_{\text{diatom}}$  record with existing data from Lakes Baikal and Kotokel, and  
129 examine regional palaeohydrology, and consider local and extrinsic mechanisms that  
130 may be driving palaeohydrological variability (Williams et al., 2011).

131 **1.1. Study Site:**

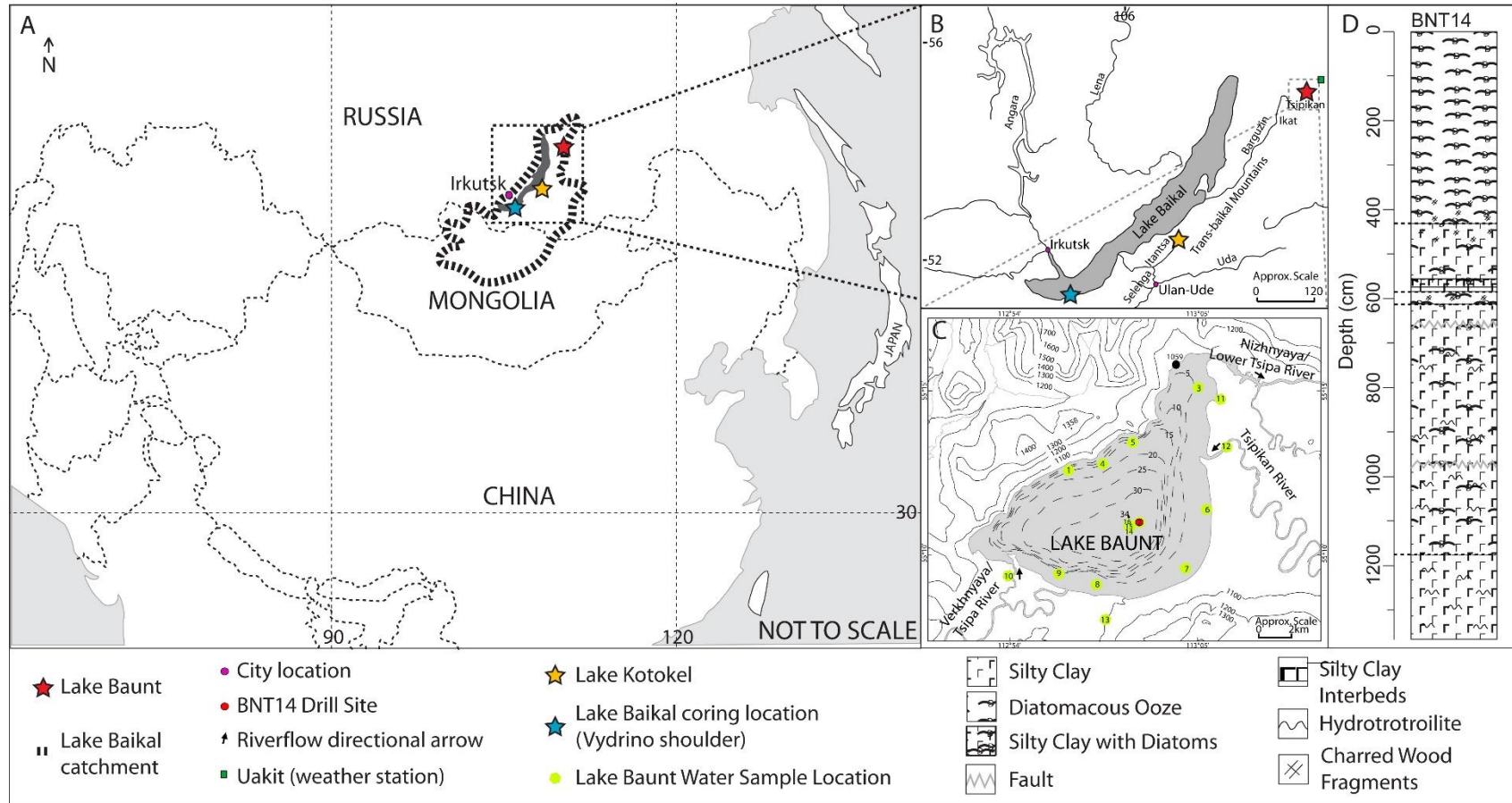
132 Lake Baunt (55°11'15"N, 113°01'45"E) is a tectonic lake (Bezrukova et al., 2017) in  
133 the Transbaikal mountains of southern Siberia, 200 km to the east of Lake Baikal's  
134 northern basin (Figure 1) and is one of the larger lakes in the Tsipikan-Baunt lake  
135 district (Shchetnikov, 2007; Yakhnenko et al., 2008). Located at ~1050 m a.s.l., Baunt  
136 has a surface area of 111 km<sup>2</sup> (19 km length on a SW-NE elongation and 9 km width),  
137 with an average depth of 17m and maximum depth of 33m (Krainov et al., 2017). The  
138 catchment predominantly lies to the south, east, and west (Krainov et al., 2017), and  
139 is bounded by the Ikat and Tsipikan highlands (Solotchin et al., 2015) (Figure 1).  
140 Glaciation in this region is limited to the Kodar range of the Transbaikal mountains  
141 (Stokes et al., 2013), and has receded recently due to anthropogenic warming, while  
142 extensive mountain glacier coverage existed during the Last Glacial (Margold et al.,  
143 2016; Martin and Jansson, 2011; Stokes et al., 2013). Baunt receives water from the  
144 Verkhnyaya (Upper) Tsipa and Tsipikan rivers (Krainov et al., 2017), and discharges  
145 into the Nizhnyaya (Lower) Tsipa River (Ufimtsev et al., 2009) (Figure 1). It is currently  
146 oligotrophic (surface water pH 7 – 7.2 (Kozhov, 1950)) and undergoes thermal  
147 stratification during the summer, but is frozen for ~8 months (October-May) (Alpat'ev  
148 et al., 1976).

149 The regional geology is predominantly the Barguzin and Vitimkan igneous granitic  
150 complexes (part of the Angara-Vitim batholith) (Nenakhov and Nikitin, 2007; Rytsk et  
151 al., 2007; Tsygankov et al., 2007). In the lake basin, Neogene-Quaternary sediments  
152 including sands, clays and gravels dominate (Bezrukova et al., 2017; Krainov et al.,  
153 2017; Shchetnikov, 2007), while Holocene sediments include lacustrine, fluvial and  
154 peat deposits (Bezrukova et al., 2017). No carbonate rocks are found within the  
155 catchment (Ryabenko et al., 1964), which sits in taiga forest, dominated by *Larix*



156 *gmelinii* (Larch) and *Pinus sylvestris* (Scots Pine). Mountain shrubs, grass and moss  
157 tundra occupy higher altitudes (Anekhonov, 1995; Müller et al., 2014).

158 Regional climate is dominated by the Siberian High anticyclone, with winter pressures  
159 reaching ~1030mb (Tubi and Dayan, 2013), but in summer, when it is inactive,  
160 pressures drop to ~1005mb. For the period between 1961-1990 CE (common era),  
161 averaged mean air temperatures at Baunt, corrected for elevation, are +15.7°C (July)  
162 and –28.4°C (January) (Leemans and Cramer, 1991). Average annual precipitation is  
163 ~400 mm (Leemans and Cramer, 1991), with the highest levels in summer (Huhne  
164 and Slingo, 2011). Precipitation is generally considered to be North Atlantic sourced  
165 recycled summertime rainfall, transported by the westerlies (Park et al., 2014; Tubi  
166 and Dayan, 2013), with a small proportion from wintertime snowfall (Huhne and Slingo,  
167 2011). However, recent work indicates the region is influenced by the Atlantic  
168 westerlies, the East Asian Monsoon, and intrusions of Arctic air (Kostrova et al., 2020;  
169 Osipova and Osipov, 2019). The relative proportion of these sources varies across the  
170 year, with winter months and transitional periods (March-April-May and September-  
171 October-November) dominated by westerly precipitation (Kostrova et al., 2020;  
172 Osipova and Osipov, 2019), while during summer, inflows from the south-west and  
173 south-east increase (Osipova and Osipov, 2019). Variations in the contribution from  
174 these sources change across the Transbaikal mountains, with southern regions being  
175 more heavily influenced by southerly sources (Osipova and Osipov, 2019).



178 **Figure 1:** (A) Schematic Map of Asia highlighting the position of Lakes Baunt, Kotokel and Baikal. Lake Baikal's catchment  
 179 area is shown. (B) Closer image of the Lake Baikal region, showing Lake Baunt alongside major rivers in the region. (C) Close image of  
 180 Lake Baunt highlighting basin topography and the regional topography. Drill location of the BNT14 core is shown alongside  
 181 locations where water samples were taken from Lake Baunt and surrounding rivers and lakes. River inflows and outflow are shown  
 182 with directional arrows. (D) Core litho-stratigraphy for BNT14 summarised from Krainov et al. (2017).

183 **2. Methodology:**

184 **2.1. Core Collection and Lithology**

185 The BNT14 core (55°11'15"N, 113°01'45"E; water depth 33m; Figure 1.C) was  
186 collected in March 2014, while the lake was frozen (maximum ice thickness of  
187 ~2m with limited movements) using a UWITEC gravity corer (Krainov et al.,  
188 2017), at the site identified to have the most uniform sedimentation rates. The  
189 UWITEC system used hammer action with inner 63 mm PVC liners to extract  
190 the 13.66 m core in 8 liners, over 3 days, with a 95% recovery rate (Krainov et  
191 al., 2017). The litho-stratigraphy consists of silty clay at the base (1366-  
192 1170cm), followed by a change to silty clay with abundant diatoms (1170-  
193 620cm). A short section of diatomaceous ooze occurs between 620-580cm,  
194 followed by a return to silty clay with diatoms. From 540cm there is a switch to  
195 diatomaceous ooze, which continues to the core top. For full description see  
196 Krainov et al. (2017) (Figure 1.D).

197 **2.2. Chronology Construction**

198 The Lake Baunt chronology is a refined version of the age model developed  
199 by Krainov et al. (2018, 2017) and is based on 15 radiocarbon dates of bulk  
200 sediments (Table 1), coupled with <sup>210</sup>Pb analyses, which attempt to constrain  
201 the upper-most sections (supplementary information).

| Sample Code  | Sample Depth (cm) | 14C age    | IntCal20 Calibrated Range |
|--------------|-------------------|------------|---------------------------|
| Poz-BNT14-52 | 52                | 5590 ± 35  | 6439-6295                 |
| UBA-32755    | 97.5              | 5049 ± 40  | 6609-6302                 |
| Poz- BNT-200 | 200               | 5775 ± 30  | 7452-6451                 |
| Poz- BNT-400 | 400               | 9000 ± 50  | 10340-9891                |
| UBA-32756    | 497.5             | 11489 ± 60 | 13497-12863               |
| Poz- BNT-600 | 600               | 11620 ± 50 | 13601-13368               |

|              |      |             |             |
|--------------|------|-------------|-------------|
| Poz-BNT-692  | 691  | 14090 ± 80  | 17403-16885 |
| Poz-BNT-800  | 800  | 14930 ± 70  | 18621-18071 |
| Poz-BNT-950  | 950  | 18220 ± 80  | 22385-21900 |
| Poz-BNT-1110 | 1110 | 18850 ± 120 | 24465-22438 |
| Poz-BNT-1150 | 1150 | 20680 ± 140 | 25328-24329 |
| Poz-BNT-1172 | 1172 | 21670 ± 140 | 26195-25703 |
| Poz-BNT-1195 | 1195 | 21720 ± 140 | 26310-25820 |
| Poz-BNT-1277 | 1277 | 24760 ± 190 | 29315-28565 |
| Poz-BNT-1350 | 1350 | 25350 ± 180 | 30000-29215 |

202 **Table 1:** AMS radiocarbon dates from the BNT14 core. Dates were  
203 calibrated using IntCal20 (Reimer et al., 2020) in OxCal 4.4.

204 The  $^{210}\text{Pb}$  profile was produced using four air dried samples from the upper  
205 10cm of the BNT14 core, which were analysed by direct gamma assay for  
206  $^{210}\text{Pb}$ ,  $^{137}\text{Cs}$ ,  $^{226}\text{Ra}$  and  $^{241}\text{Am}$  using an ORTEC HPGe GWL series well-type  
207 coaxial low background intrinsic germanium detector, at the Environmental  
208 Radiometric Facility at University College London.  $^{210}\text{Pb}$  was determined from  
209 gamma emission at 46.5keV, while  $^{226}\text{Ra}$  was determined by the 295keV and  
210 352keV gamma rays, re emitted by its daughter isotope  $^{214}\text{Pb}$ , following 3  
211 weeks storage in sealed containers, allowing radioactive equilibration  
212 (Appleby et al., 1986).  $^{137}\text{Cs}$  and  $^{241}\text{Am}$  were determined by their emissions at  
213 662keV and 59.5keV (Appleby et al., 1986). Detector efficiencies were  
214 measured using calibrated sourced and sediment samples of known activity,  
215 with corrections being made for the effect of self-absorption of low energy  
216 gamma rays within the sample (Appleby, 2002).

217 The chronological information (Table 1) has undergone Bayesian age  
218 modelling in OxCal 4.4 to produce a *P\_Sequence* depositional model (Bronk  
219 Ramsey, 2008; Bronk Ramsey, 2009a; Bronk Ramsey, 2009b), within which,  
220 radiocarbon dates were calibrated using the IntCal20 curve (Reimer et al.,

221 2020). The model incorporates automatic outlier detection using the general  
222 model (Bronk Ramsey, 2009b) with interpolation between dates allowing for  
223 sedimentological changes between dated points (Bronk Ramsey and Lee,  
224 2013). A boundary, which is a Bayesian function to recognise differences  
225 between sedimentary or chronological units within a sequence, has been  
226 incorporated into the model during a period of sediment source change,  
227 identified in the core lithostratigraphy (see Krainov et al., 2018, 2017).

228 To facilitate comparison between regional lake records, chronological records  
229 from lakes Baikal (composite chronology for cores CON01-605-5 and CON01-  
230 605-3 from the Vydrino Shoulder) and Kotokel (core KTK2) were re-modelled  
231 using IntCal20 (Reimer et al., 2020), as previous studies used different  
232 calibration curves, IntCal09 and CalPal07\_Hulu respectively (Bezrukova et al.,  
233 2010; Mackay et al., 2011), with different underlying data and statistical  
234 treatment of the calibration information (e.g. Reimer et al., 2009; Weninger  
235 and Jöris, 2008). Models were produced following the same method as  
236 described above for Lake Baunt. Furthermore, in this study, the Lake Kotokel  
237 age model does not include dates transferred from the Lake Sihailongwan  
238 record (42° 17'N, 126° 36'E) (Bezrukova et al., 2010; Stebich et al., 2009) due  
239 to the large distance between the two sites, which could introduce monsoonal  
240 influences into the regional comparison. The approach of using only locally  
241 derived chronological information is undertaken to ensure the three records  
242 can be compared independently to each other, to build up a picture of regional  
243 palaeohydrological change.

244 **2.3. Diatom analyses**

245 Diatom composition analyses were undertaken across the BNT14 core.  
246 Samples were prepared following the digestion procedure of Battarbee et al.,  
247 (2001) (supplementary information). Diatom analyses were converted to  
248 relative proportions (%), concentrations and diatom fluxes (supplementary  
249 information). Diatom dissolution was quantified for the dominant taxa, with  
250 individual frustules being classified into 1 of 4 stages: (1) pristine, (2) little  
251 dissolution, (3) very dissolved, and (4) almost unrecognisable. Dissolution  
252 stages were converted to a dissolution  $F_{\text{index}}$  (Ryves et al., 2001: Flower  
253 and Ryves 2009), using the observations above to determine a ratio of pristine  
254 valves against total counts, expressed as:

255 
$$F_i = \sum_j^m n_{ij} / \sum_j^m N_j$$

256 **Equation 1:  $F_{\text{Index}}$**

257 Where  $F_i$  is the  $F_{\text{index}}$  for sample  $i$ ,  $n$  is the sum of the pristine valves for  
258 species  $j$  in the sample, and  $N$  is the sum of the total number of valves in the  
259 same sample.

260 **2.4. Isotope analyses**

261 **2.4.1. Water samples**

262 In 2014 and 2016, water samples were collected from Lake Baunt and its  
263 fluvial inflows, and a small nearby lake. Samples were collected in spring (23-  
264 Mar-2014;  $n=3$ , 27-Mar-2016;  $n=1$ , 30-Mar-2016;  $n=2$ ), while the lake was  
265 frozen, and during summer, post ice melt (21-Aug-2014;  $n=6$ ). Hydrogen and  
266 oxygen isotope analysis was conducted at the Isotope Laboratory (AWI  
267 Potsdam) with a Finnigan MAT Delta-S mass spectrometer using equilibration

268 techniques. Internal  $1\sigma$  errors was better than  $\pm 0.8\text{‰}$  for  $\delta\text{D}$  and  $\pm 0.1\text{‰}$  for  
269  $\delta^{18}\text{O}$  (Meyer et al., 2000).

#### 270 **2.4.2. $\delta^{18}\text{O}_{\text{diatom}}$ analyses**

271 In total, 59 cleaned samples were chosen from the BNT14 core to cover the  
272 transition from the Late Pleistocene and the period of instability documented  
273 in the Early Holocene (Blockley et al., 2018; Rasmussen et al., 2014). The  
274 samples were purified prior to analysis following published procedures (e.g.  
275 Brewer et al., 2008; Leng and Marshall, 2004), to exclude other oxygen  
276 bearing components (Morley et al., 2004; van Hardenbroek et al., 2018).  
277 Cleaning of the Lake Baunt samples followed Morley et al. (2004). Primarily,  
278 samples underwent a step-wise removal of organic matter using hydrogen  
279 peroxide ( $\text{H}_2\text{O}_2$ ) and hydrochloric acid (HCl), before being sieved over a  $5\ \mu\text{m}$   
280 mesh to remove clay particles. After this, samples underwent a three-stage  
281 heavy liquid separation using sodium polytungstate ( $3\text{Na}_2\text{WO}_4 \cdot 9\text{WO}_3 \cdot \text{H}_2\text{O}$ ).  
282 Finally samples were cleaned with a nitric/perchloric acid mixture  
283 ( $\text{HNO}_3:\text{HClO}_4$ ) and dried (Morley et al., 2004).

284 Sample purity was assessed using scanning electron microscopy (SEM)  
285 (Earth Sciences Department, University College London) and electron  
286 microprobe X-ray analysis (EMPA; Reed, 2005) with a microprobe JXA-8200  
287 (JEOL Ltd, Japan) at the Shared-Use Analytical Centre of the IGC SB RAS, to  
288 estimate the remaining contaminants, particularly silt quantities, prior to  
289 analysis, to allow them to be used for the mass-balance correction. For EMPA,  
290 less than 1 mg of purified diatom material was placed on carbon-tabs mounted  
291 on duralumin substrate, and carbon coated. Analytical spectra were registered

292 and processed automatically by the EDS Semi-Quantitative Analysis software  
293 of the energy-dispersive spectrometer EX-84055MU (JEOL Ltd, Japan).  
294 Quantitative analysis was performed using the standardless procedure (all  
295 detectable elements displayed as oxides normalised to 100% weight); with  
296 results expressed as weight percentages (Pavlova et al., 2014).

297 The oxygen isotope analysis was undertaken at the National Environmental  
298 Isotope Facility, British Geological Survey, Keyworth, UK. Samples were  
299 prepared for analysis using a step-wise fluorination method (see Leng and  
300 Sloane (2008)), where, firstly, samples were 'outgassed' (dehydrated) at room  
301 temperature in nickel reaction vessels to remove loosely bound water.  
302 Secondly, samples underwent pre-fluorination, involving a stoichiometric  
303 deficiency of the reagent (bromine pentafluoride, BrF<sub>5</sub>) at 250°C (Leng and  
304 Sloane, 2008), to remove loosely bound water and the hydroxyl layer. This is  
305 necessary as this outer hydrous layer is freely exchangeable and does not  
306 reflect the isotopic composition of the frustule at the time of burial (Leng and  
307 Barker, 2006). Finally, the samples were fully reacted at 500°C for 16 hours in  
308 an excess of reagent, and the liberated oxygen is separated from waste  
309 products using liquid nitrogen, purified using two additional waste traps cooled  
310 using liquid nitrogen, and converted to CO<sub>2</sub> by exposure to a graphite rod at  
311 ~650°C (Leng and Sloane, 2008). Once converted, the gas yield was  
312 calculated using a calibrated capacitance manometer and the CO<sub>2</sub> is collected  
313 under liquid nitrogen for analysis. The CO<sub>2</sub> produced was analysed using a  
314 Finnegan MAT253 dual inlet isotope ratio mass spectrometer. Isotope results  
315 are reported in delta (δ) notation in per mille (‰) and were calibrated to the  
316 VSMOW scale using a laboratory reference material of known δ<sup>18</sup>O (BFC =



317 +28.9 ‰ VSMOW) relative to the international standard NBS 28. Analytical  
318 reproducibility of BFC for this dataset was  $\pm 0.2$  ‰.

319 Despite the intensive cleaning process, some samples contained small levels  
320 of contaminants (average of around 6% contaminant), particularly due to their  
321 ability to become electro-statically charged to the diatom frustules (Brewer et  
322 al., 2008). To compensate for contaminants potentially affecting the Lake  
323 Baunt  $\delta^{18}\text{O}_{\text{diatom}}$  record, a mass balance correction was applied to the original  
324 data, following Swann and Leng (2009). Initially the percentage silt was  
325 established (equation 2):

$$326 \quad \% \text{Silt Contamination} = (\text{sample Al} / \text{silt Al}) * 100$$

327 **Equation 2: %silt.**

328 Where sample Al is the EDS-measured  $\text{Al}_2\text{O}_3$  and silt Al is the average  $\text{Al}_2\text{O}_3$   
329 for terrigenous samples during EDS analysis. Once this was established, a  
330 mass balance correction was applied (equation 3).

$$331 \quad \delta^{18}\text{O}_{\text{corrected}} = (\delta^{18}\text{O}_{\text{measured}} - (\% \text{Silt Contamination} / 100)) * \delta^{18}\text{O}_{\text{contamination}} /$$
$$332 \quad (\% \text{purity} / 100)$$

333 **Equation 3: mass balance correction.**

334 where  $\delta^{18}\text{O}_{\text{corrected}}$  is the measured value after it has been corrected for  
335 contaminants,  $\delta^{18}\text{O}_{\text{measured}}$  is the original measured value, %Silt Contamination  
336 is the percentage of the known contaminant ( $\text{Al}_2\text{O}_3$ ), established from EDS  
337 measurements, while %purity is the percentage of diatom material,  
338 established by geochemical methods (Swann and Leng, 2009). Silt samples  
339 were obtained by dissolving diatoms from 4 samples in NaOH and retaining

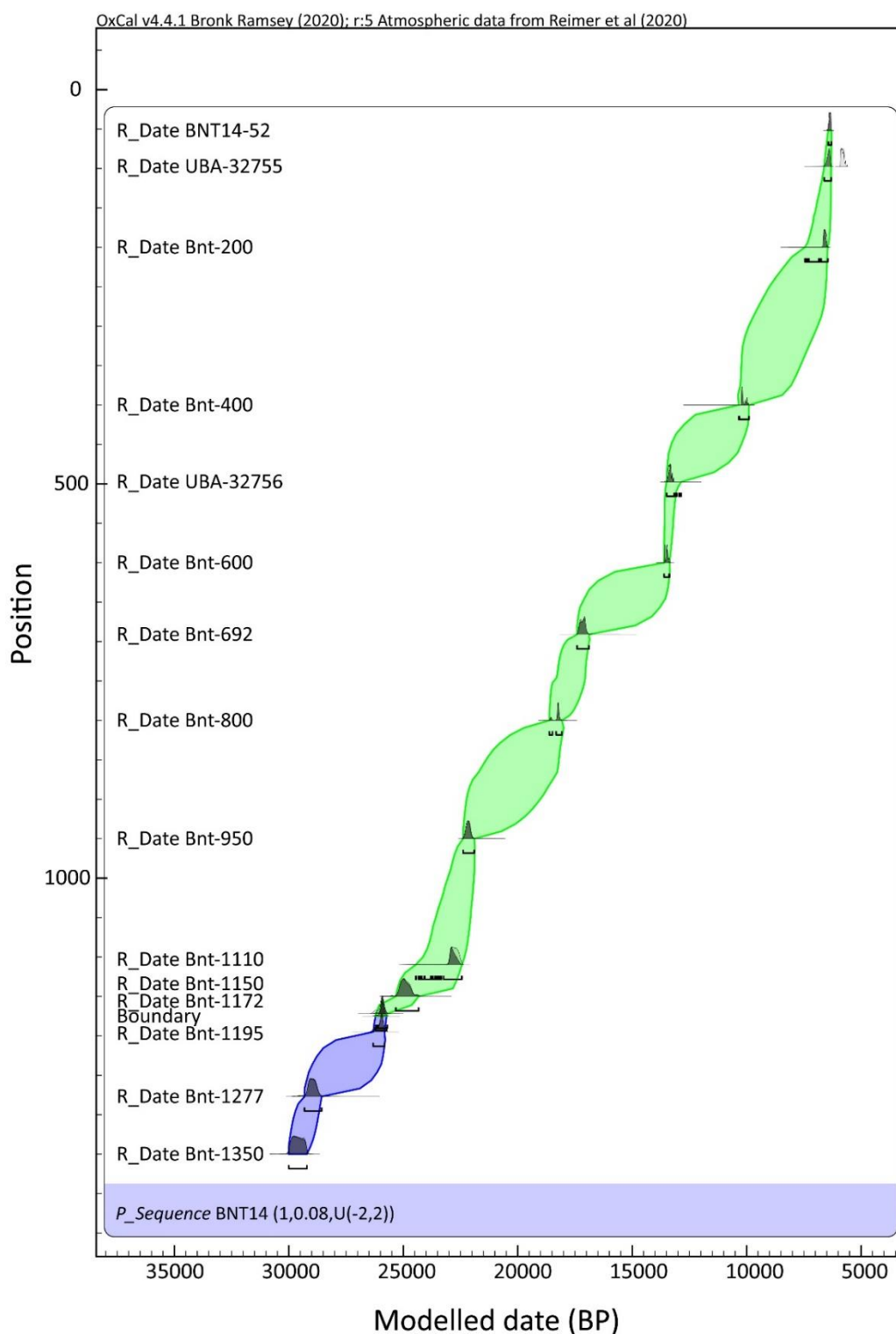
340 the residues that included material in the size fractions between ~5-63 $\mu\text{m}$ .  
341 These end members were used to create a signal end member  $\delta^{18}\text{O}_{\text{silt}}$  value  
342 of +10.34‰, (Swann and Patwardhan, 2011).

### 343 **3. Results:**

#### 344 **3.1. Age model**

345 The full age model for Baunt (Figure 2) only has minor changes from Krainov  
346 et al. (2018, 2017) in most places, with the addition of new dating information  
347 (additional radiocarbon dates and  $^{210}\text{Pb}$  data). The biggest differences include  
348 that outlier detection has down-weighted one new date, UBA-32755, as a  
349 potential outlier, and that the top of the core is now placed around ~6.2 ka cal  
350 BP based on new radiocarbon dates, supported by the  $^{210}\text{Pb}$  profile, which  
351 demonstrated BNT14 had little unsupported  $^{210}\text{Pb}$  activity, and additionally,  
352 artificial fallout radionuclides for  $^{137}\text{Cs}$  and  $^{241}\text{Am}$ , were not identified  
353 (supplementary information). This indicates BNT14 does not contain  
354 sediments deposited during the past 100-150 years, and alongside the  
355 radiocarbon evidence, suggests that there is a potential hiatus from ~6 ka cal  
356 BP, or that the upper section of BNT14 was lost during coring, due to difficult  
357 conditions. A rapid rise in sedimentation rate between 600 and 500 cm, is  
358 indicative of changes occurring within the lake, which are documented as  
359 variations in the lithostratigraphy (Figure 1.D). These highlight a shift to  
360 diatomaceous ooze between 620-580cm, followed by a return to silty clay with  
361 diatoms at 580cm and a switch back to diatomaceous ooze from 540cm, and  
362 therefore, these sedimentation rate variations are linked to periods of  
363 increased diatom productivity within the lake, increasing the quantity of  
364 diatoms persevered in the sediments, alongside increased organic materials

365 from the wider landscape following afforestation in the late-glacial interstadial  
366 (Tarasov et al., 2007, 2009).



367

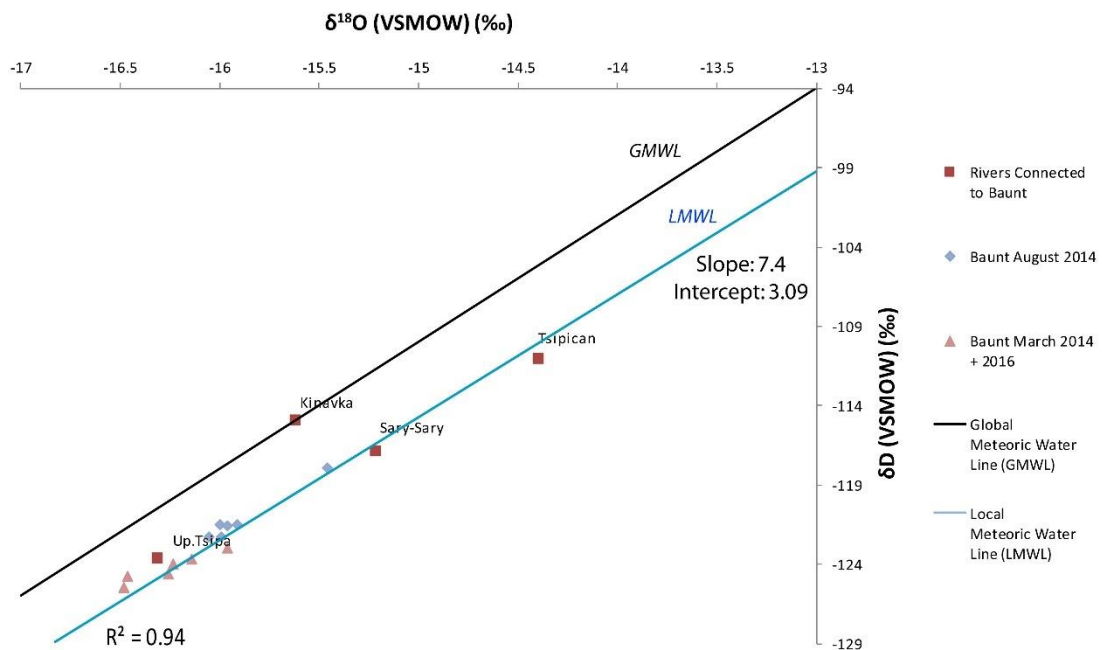
368 **Figure 2:** Bayesian *P\_sequence* depositional Age model for Lake Baunt  
369 incorporating 15  $^{14}\text{C}$  dates calibrated using IntCal20 (Reimer et al., 2020),  
370 and modelled in OxCal 4.4.

371 The updated age model for Lake Baikal is consistent with the previous age model for  
372 the majority of the Holocene (Mackay et al., 2011) (supplementary information),  
373 however, earliest Holocene and Younger Dryas sections are now inferred to be slightly  
374 older (by ~100-150 years), but still within the errors on the two chronologies. This is  
375 due to the close similarity between the IntCal09 and IntCal20 radiocarbon calibration  
376 curves for the Holocene period, as both curves are based on tree ring data sets  
377 (Reimer et al., 2009, 2020). This is similar for Lake Kotokel, where most of the updated  
378 model is similar to that of Bezrukova et al. (2010) (supplementary information), again  
379 linked to the use of tree rings for the upper sections of the calibration curve (Weninger  
380 and Jöris, 2008). However, in the section of the core between ~11.6 and ~7.0 ka cal  
381 BP the two models differ, with the largest variation seen at 424cm, with a difference of  
382 ~1000 years (~10.6 ka cal BP in the original chronology and ~9.5 ka cal BP in the  
383 updated chronology) (Bezrukova et al., 2010). These differences are explained by the  
384 different tuning approaches taken between the two age models, with the published  
385 Bezrukova et al. (2010) model having a shift in the modelled sedimentation rates for  
386 Kotokel, through the addition of the transferred age of ~10.6 ka cal BP, based on  
387 dating and pollen information from Lake Sihailongwan (42° 17'N, 126°  
388 36'E)(Bezrukova et al., 2010; Stebich et al., 2009), while the revised model used here  
389 has linear sedimentation through this section of the core. As discussed above, in this  
390 study, only local dating information has been used in the revised age model, so that  
391 we can robustly investigate regional palaeohydrology. The oxygen isotope curves for  
392 lakes Baikal and Kotokel are plotted on both the previously published, and revised age  
393 models for clarity (section 4).

394 **3.2. The isotope composition of modern waters**

395 The average  $\delta^{18}\text{O}$  value from Lake Baunt waters is  $-16.0\text{‰}$ , with slightly higher  
 396 average values during the summer ( $-15.9\text{‰}$ ) than under ice ( $-16.3\text{‰}$ ). Figure 3 shows  
 397 that although average  $\delta^{18}\text{O}$  values are similar, there is a small seasonal variation  
 398 (Figure 3). Rivers flowing into Baunt have a range of  $\delta^{18}\text{O}$  between  $-14.49\text{‰}$  and –  
 399  $16.31\text{‰}$ , with greatest similarity seen between the Upper Tsipa river and Baunt. River  
 400 water temperatures vary substantially, from  $5^{\circ}\text{C}$  to  $19.6^{\circ}\text{C}$ , despite only being taken  
 401 over 3 days during the summer period (August). All the data lie on the local meteoric  
 402 water line, except one river.

403



404

405 **Figure 3:**  $\delta^{18}\text{O}$ - $\delta\text{D}$  diagram for the Lake Baunt and nearby water sources against the  
 406 Global Meteoric Water Line (GMWL).

### 407 3.3. $\delta^{18}\text{O}_{\text{diatom}}$ record

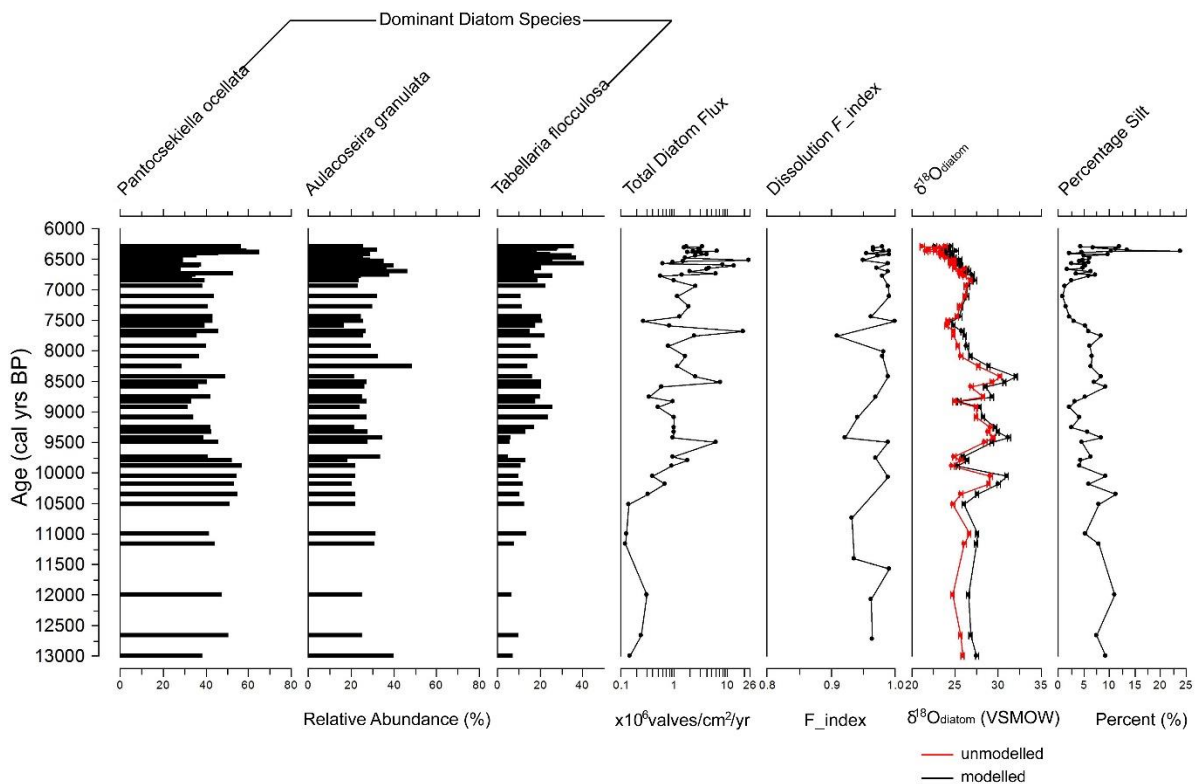
408 Samples have undergone a mass balance correction (section 2.4.2) to compensate  
409 for any remaining contaminants and hereafter, all  $\delta^{18}\text{O}_{\text{diatom}}$  values refer to the  
410 corrected  $\delta^{18}\text{O}_{\text{diatom}}$  data. The Baunt isotope record covers ca. 13.0 to 6.2 ka cal BP,  
411 and shows several distinct shifts.  $\delta^{18}\text{O}_{\text{diatom}}$  values range from +22.7‰ to +32.1‰  
412 (Figure 4), with a general transition to lower  $\delta^{18}\text{O}_{\text{diatom}}$  values of around 4‰ from the  
413 Early to Mid Holocene. The earliest section of the record from ca. 13.0 to 10.5 ka cal  
414 BP documents low amplitude  $\delta^{18}\text{O}_{\text{diatom}}$  change between +25.9 and +27.6‰ (Figure  
415 4), with the largest reduction at ~10.5 ka cal BP being greater than analytical error  
416 (0.2‰). Following this, the record shows large peaks and troughs, with values  
417 reaching over +31.0‰ between ~10.0 ka cal BP and ~8.4 ka cal BP, interrupted by  
418 transitions to lower  $\delta^{18}\text{O}_{\text{diatom}}$  values of +25.3‰ at ~9.8 ka cal BP and +25.5‰ at ~8.8  
419 ka cal BP (although the lowest value of this decline is only recorded in one sample).  
420 After the final high value at ~8.4 ka cal BP, the  $\delta^{18}\text{O}_{\text{diatom}}$  abruptly drops to +26.8‰ by  
421 ~8.1 ka cal BP and then continues to decline to +24.5‰ at ~7.5 ka cal BP. After this,  
422 values increase to +27.2‰ by ~6.9 ka cal BP and then gradually decline from +27.0‰  
423 to +24.5‰ by the end of the record at ~6.2 ka cal BP.

### 424 3.4 Summary diatom record

425 The most dominant diatom species, *Aulacoseira granulata* (Ehrenberg) Simonsen,  
426 *Pantocsekiella ocellata* (Pantocsek) K.T.Kiss and E.Ács and *Tabellaria*  
427 *flocculosa* (Roth) Kützing, found in BNT14 (Figure 4) show limited change across the  
428 studied section, although *T. flocculosa* does increase in compositional importance  
429 from the Younger Dryas (~10%) to the Mid Holocene (up to ~40%)(supplementary  
430 information). Sampling resolution matches the  $\delta^{18}\text{O}_{\text{diatom}}$  samples and ranges from

431 samples every ~600 (Younger Dryas time period) to ~20 years (Mid-Holocene). All  
 432 species are considered to be planktonic and represent the same environment. Total  
 433 diatom flux is lower at the base of the start of the record and rises at ~10.5 ka cal BP,  
 434 where after it fluctuates, while  $F_{index}$  values are always above 0.9, which indicate  
 435 that dissolution within the samples is very limited.

436



437 **Figure 4:** Summary diatom data showing percentage abundance of the three-  
 438 dominant species against the Total Diatom Flux (shown on a logarithmic scale),  
 439 with Dissolution  $F_{index}$  scores, alongside the unmodelled and modelled  
 440 (corrected)  $\delta^{18}O_{diatom}$  and the percentage silt. Plotted in C2 (Juggins, 2016).  
 441  
 442

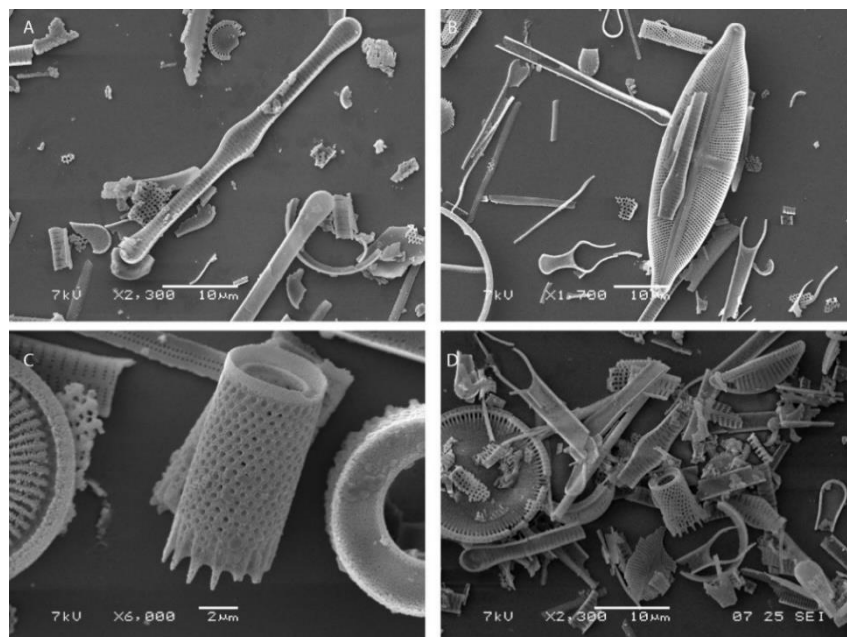
443 **4. Discussion:**

444 **4.1. Integrity of and controls on the new Lake Baunt  $\delta^{18}O_{diatom}$**

445 **palaeolimnological record**

446 Several factors can potentially complicate interpretation of  $\delta^{18}O_{diatom}$  data from  
 447 palaeolimnological records, including contamination from other sedimentary oxygen-  
 448 bearing minerals (e.g. clays, silts and tephras)(Brewer et al., 2008; Wilson et al.,

449 2014), vital effects (van Hardenbroek et al., 2018), and taphonomic processes such  
450 as diatom dissolution (Smith et al., 2016). To account for potential contamination, we  
451 mass-balanced remodelled  $\delta^{18}\text{O}_{\text{diatom}}$  values based on  $\text{Al}_2\text{O}_3$  as an estimator of  
452 contamination (Brewer et al., 2008), after having undertaken standard diatom  
453 purification procedures (Mackay et al., 2011; Morley et al., 2004; Wilson et al., 2014)  
454 (Figure 5). Previous work suggests that vital and species effects on lacustrine diatoms  
455 are within analytical error (Swann et al., 2010, 2007; van Hardenbroek et al., 2018),  
456 however for Baunt vital effects are unlikely to be an issue because the same three  
457 planktonic species persist throughout the record, with relatively little variation (Figure  
458 4). Diatom dissolution can alter  $\delta^{18}\text{O}_{\text{diatom}}$ , causing a small negative effect (ca. 0.6‰)  
459 beyond analytical error (Smith et al., 2016), but the influence of diatom dissolution in  
460 Baunt is also considered to be minimal, due to the excellent preservation of diatoms  
461 across the whole core, with persistent  $F_{\text{index}}$  values of above 0.9 (where higher  
462 values on the 0-1 scale indicate lower dissolution) (Figure 4; supplementary  
463 information).



464



465 **Figure 5:** Scanning Electron Microscopy Images of cleaned isotope samples from  
466 varying Lake Baunt Depths: (A) 0.05m, (B) 1.90m, (C) 3.75m, (D) 4.20m.

467 As an open lake, and with no evidence of species effects or dissolution on the  
468 remodelled  $\delta^{18}\text{O}_{\text{diatom}}$  record, it is expected that Baunt's  $\delta^{18}\text{O}_{\text{diatom}}$  record will reflect  
469 changes in temperature and palaeohydrology, linked to  $\delta^{18}\text{O}_{\text{precipitation}}$  values (Leng and  
470 Barker, 2006; Leng and Marshall, 2004; Leng and Swann, 2010). The Baunt  $\delta^{18}\text{O}_{\text{diatom}}$   
471 record has a range in values of 9.4‰, and if these were driven purely by changes in  
472 the lake water temperature, it indicates temperature changes through this period that  
473 appear unrealistic. This is because the Dansgaard temperature dependence  
474 relationship suggests that for every 1°C air temperature increase the  $\delta^{18}\text{O}_{\text{precipitation}}$   
475 value only increases by +0.50‰ in Irkutsk (Kostrova et al., 2020). Alongside the air  
476 temperature fractionation, the diatom silica to water fractionation gradient is  $-0.2\text{‰}/\text{°C}$   
477 (Dodd and Sharp, 2010; Leng and Barker, 2006), and combined, these cause a +0.3‰  
478 increase in  $\delta^{18}\text{O}_{\text{diatom}}$ , for every 1°C air temperature increase. This would, therefore,  
479 suggest that to drive the change of 9.4‰ seen across the Baunt record, a change of  
480  $\sim 31.3\text{°C}$  in air temperature is needed. As a result of this, it is anticipated that the  
481 influence of temperature on the  $\delta^{18}\text{O}_{\text{diatom}}$  record is limited and other drivers are  
482 involved, with changes in  $\delta^{18}\text{O}_{\text{lakewater}}$  potentially related to variations in  $\delta^{18}\text{O}_{\text{precipitation}}$   
483 and/or the hydrological conditions as determined by several previous studies (e.g.  
484 Cartier et al., 2019; Kostrova et al., 2019, 2013b; Meyer et al., 2015). The  $\delta^{18}\text{O}_{\text{lakewater}}$   
485 samples from Baunt provide important information on the modern lake. The average  
486 Baunt  $\delta^{18}\text{O}_{\text{lakewater}}$  is  $-16.0\text{‰}$ , with limited range, both across the lake and between  
487 surface and bottom water (Figure 3), highlighting it is well mixed. The  $\delta^{18}\text{O}_{\text{lakewater}}$  is  
488 similar to the annual averaged  $\delta^{18}\text{O}_{\text{precipitation}}$  value of  $-15.0\text{‰}$  calculated for the BNT14  
489 core location (Bowen, 2020; Bowen et al., 2005). This is important as it is essential for

490 the  $\delta^{18}\text{O}_{\text{lakewater}}$  to have averaged out local/seasonal  $\delta^{18}\text{O}$  variations in precipitation  
491 (Leng and Marshall, 2004), although the small differences between March and August  
492 values highlight a minor seasonal influence. The  $\delta^{18}\text{O}_{\text{lakewater}}$  and  $\delta\text{D}_{\text{lakewater}}$  values are  
493 linearly correlated, with a slope of 7.4, and lie on the local meteoric water line (Figure  
494 3), indicating that, at present, evaporation does not have a significant affect, although  
495 we cannot discount evaporation having greater influence in the past.

496

497 Given the location of Lake Baunt and its catchment, the influence of several different  
498 atmospheric circulation systems controlling varying proportions of moisture from the  
499 different source regions, likely drives changes in  $\delta^{18}\text{O}_{\text{precipitation}}$  and consequently in  
500  $\delta^{18}\text{O}_{\text{lakewater}}$ . Changes in the strength of the Siberian High will also be important, with  
501 periods of increased strength reducing the overall summer precipitation levels and  
502 increasing the proportion of snowmelt entering the lake waters (Park et al., 2014; Tubi  
503 and Dayan, 2013), while during periods of weaker Siberian High, summer precipitation  
504 is proportionally more important. The varying proportion of snowmelt is also important,  
505 as the  $\delta^{18}\text{O}_{\text{snow}}$  has much lower values (suggested  $\delta^{18}\text{O}_{\text{snow}}$  of  $-29.1\text{‰}$  and  $-41.4\text{‰}$ ;  
506 data from Chizhova et al. (2015) and Kostrova et al. (2020) respectively), than the  
507 current summer (JJA)  $\delta^{18}\text{O}_{\text{precipitation}}$  values, which range between  $\sim -12.8\text{‰}$  (Chizhova  
508 et al., 2015) and  $\sim -4.0\text{‰}$  (Kostrova et al., 2020), and thus, changed proportions of  
509 these will influence the  $\delta^{18}\text{O}_{\text{lakewater}}$  values and consequently the  $\delta^{18}\text{O}_{\text{diatom}}$  values.

510

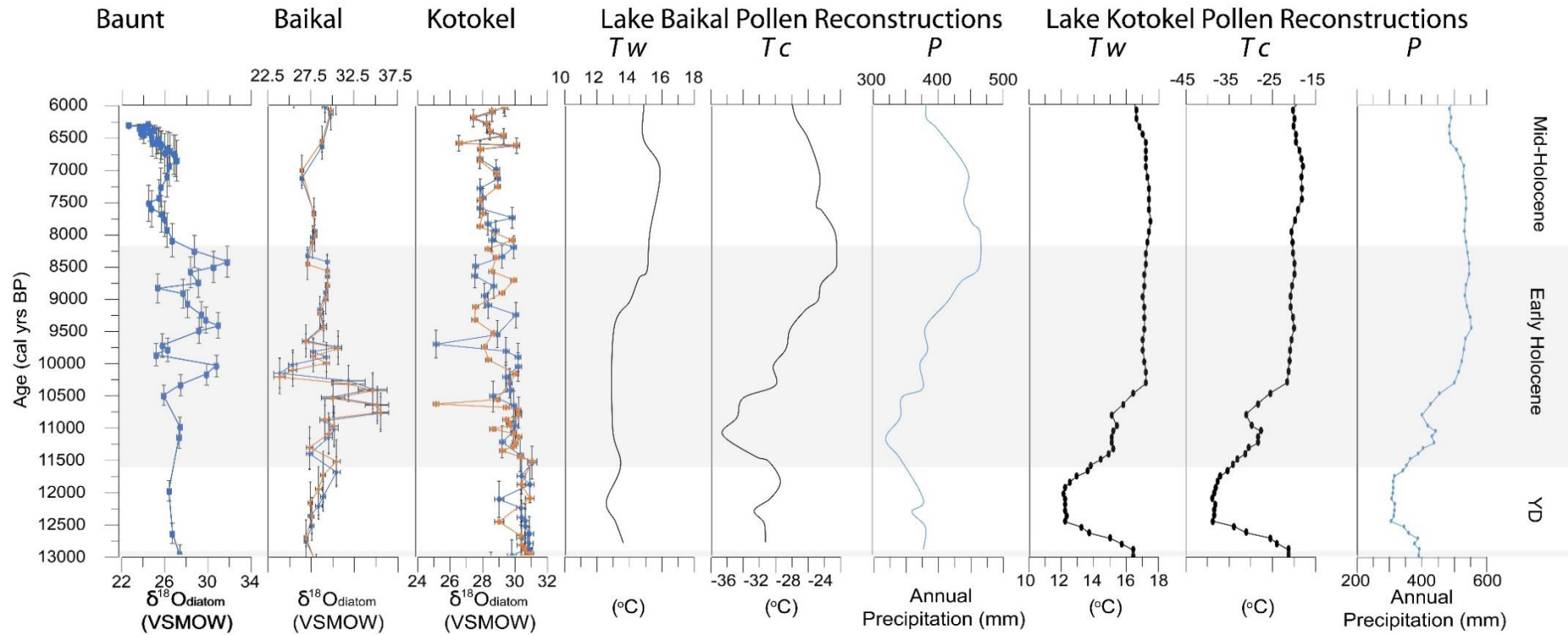
511 Similar controls are also important for driving changes in the Lake Baikal  $\delta^{18}\text{O}_{\text{diatom}}$   
512 record as in Lake Baunt, with the different proportions of precipitation coming from  
513 different source regions being a driver of changes in the  $\delta^{18}\text{O}_{\text{lakewater}}$ , while Siberian  
514 High strength changes will also influence the proportional importance of summer or

515 winter precipitation. In Baikal, changes in Siberian High strength are seen to trigger  
516 variations in the proportion of lake water coming from southern or northern rivers in its  
517 catchment, with increased proportions of snowmelt fed northern rivers when the  
518 Siberian High is strong and summer precipitation is limited. Glacier melting is also an  
519 important influence, particularly for the Vydrino cores, as these are taken off-shore  
520 from glaciers which flowed into Lake Baikal during the Younger Dryas and Early  
521 Holocene (Mackay et al., 2011). Like snowmelt, glacial meltwaters have lower  $\delta^{18}\text{O}$   
522 values than summertime  $\delta^{18}\text{O}_{\text{precipitation}}$ , and thus, increased meltwaters can have  
523 substantial influences on the  $\delta^{18}\text{O}_{\text{lakewater}}$ .

524

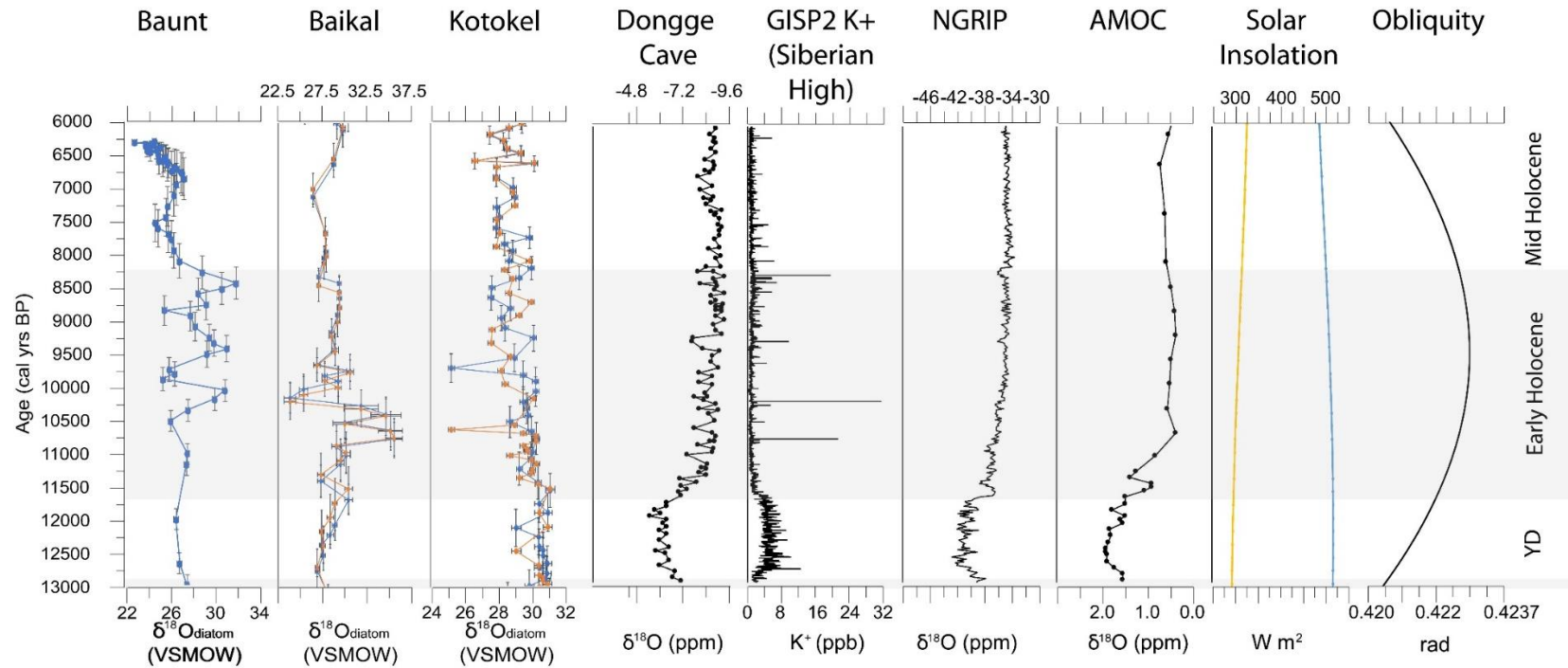
525 Changes in  $\delta^{18}\text{O}_{\text{diatom}}$  values from Kotokel are thought to be due to variations in the  
526  $\delta^{18}\text{O}_{\text{lakewater}}$  in response to changes in air temperature, hydrology and atmospheric  
527 circulation (Kostrova et al., 2016). Variations in the proportion of summer precipitation  
528 from different source regions are implicated in changes to the  $\delta^{18}\text{O}_{\text{diatom}}$  throughout  
529 the Holocene, with an increased share of precipitation from southern sources during  
530 the Early Holocene, with a shift to more Atlantic sourced moisture during the Mid-Late  
531 Holocene (Kostrova et al., 2016). Additionally, as a large but shallow lake, evaporation  
532 may also be a feature, although during the studied time period, this will be less  
533 influential than during its older history, when the lake was a closed basin, and thus,  
534 more strongly influenced by evaporation (Leng and Barker, 2006).

535



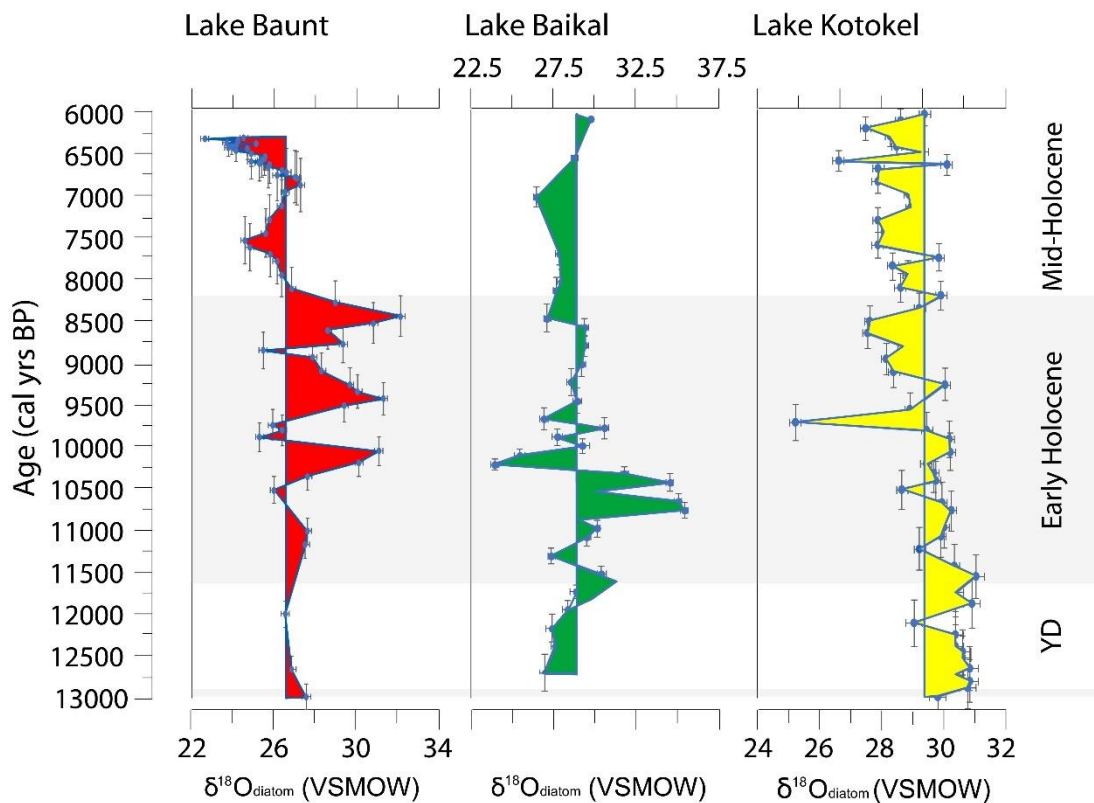
537  
538

539 **Figure 6:** Lake Baunt  $\delta^{18}\text{O}_{\text{diatom}}$  (VSMOW ‰) (shown with chronological and analytical errors) alongside  $\delta^{18}\text{O}_{\text{diatom}}$  records  
 540 (VSMOW ‰) from Lake Baikal (blue line, revised age model (this study), orange line, previous chronology (Mackay et al., 2011))  
 541 and Lake Kotokel (blue line, Siberian information age model (this study), orange line Bezrukova et al. (2010) chronology with  
 542 transferred Lake Sihailongwan ages (Kostrova et al., 2013b, 2014, 2016) (both shown with analytical errors, chronological errors  
 543 shown on revised model (blue)). Shown alongside Lake Baikal (Tarasov et al., 2007) and Lake Kotokel (Tarasov et al., 2009) pollen  
 544 reconstructions:  $T_w$  (°C)(warmest month),  $T_c$  (°C)(coldest month) (3 point running averages) and  $P$  pollen annual precipitation  
 545 reconstruction (mm)(3 point running average) (Tarasov et al., 2007, 2009).



546  
547

548 **Figure 7:** Lake Baunt  $\delta^{18}\text{O}_{\text{diatom}}$  (VSMOW ‰) (shown with chronological and analytical errors) alongside  $\delta^{18}\text{O}_{\text{diatom}}$  records  
 549 (VSMOW ‰) from Lake Baikal (blue line, revised age model (this study), orange line, previous chronology (Mackay et al., 2011))  
 550 and Lake Kotokel (blue line, Siberian information age model (this study), orange line Bezrukova et al. (2010) chronology with  
 551 transferred Lake Sihailongwan ages (Kostrova et al., 2013b, 2014, 2016) (both shown with analytical errors, chronological errors  
 552 shown on revised model (blue)). Also shown alongside Dongge Cave speleothem  $\delta^{18}\text{O}$  (‰) record (Dykoski et al., 2005), GISP2 K+  
 553 signal (ppb) (Siberian High strength) (Mayewski et al., 2004), NGRIP  $\delta^{18}\text{O}$  signal (‰) (Greenland air temperature) (Rasmussen et  
 554 al., 2014),  $\delta^{18}\text{O}_{G.inflata}$  record (‰) (AMOC strength) (McManus et al., 2004), Solar Insolation from 55°N ( $\text{W m}^2$ ) for May-June (blue  
 555 line) and August-September (yellow line) (Laskar et al., 2004) and obliquity (Laskar et al., 2004). Plotted in C2 (Juggins, 2016).



556

557 **Figure 8:** Lake Baunt  $\delta^{18}\text{O}_{\text{diatom}}$  (VSMOW ‰) (shown with chronological and  
 558 analytical errors) alongside  $\delta^{18}\text{O}_{\text{diatom}}$  records (VSMOW ‰) from Lake Baikal  
 559 (Mackay et al., 2011) and Lake Kotokel (Kostrova et al., 2013b, 2014,  
 560 2016)(shown with analytical and chronological errors). All profiles are shown  
 561 as variations from their mean isotopic value.

## 562 4.2 Palaeohydrology of Lake Baunt and Southern Siberia

### 563 4.2.1 Palaeohydrology during the Younger Dryas in Lake Baunt and Southern 564 Siberia (~12.4-11.7 ka cal BP)

565 Contrary to expectations, the Younger Dryas stadial does not show  
 566 significantly lower  $\delta^{18}\text{O}_{\text{diatom}}$  values than the Holocene, and are similar to the  
 567 mean for the whole record (Figures 4, 6, 7 and 8). Several factors may explain  
 568 this, including the seasonality of the diatom record, as the isotopic signal is  
 569 recorded during the growing season (Leng and Swann, 2010), with bulk  
 570 samples tending to be averaged across the spring to the autumn. This  
 571 indicates that the diatoms will be recording the spring-autumn conditions.

572 Under modern conditions, seasonal variations in the  $\delta^{18}\text{O}_{\text{lakewater}}$  values are  
573 small. However, during the Younger Dryas, obliquity was increasing (Figure  
574 7), causing stronger seasonality in southern Siberia (Bush, 2005). This  
575 increased seasonality may have amplified the currently small seasonal  
576 variations in the  $\delta^{18}\text{O}_{\text{lakewater}}$  values, and could explain the limited differences  
577 ( $\sim 1\text{-}2\text{‰}$ ) between the  $\delta^{18}\text{O}_{\text{diatom}}$  values for the Younger Dryas and Early  
578 Holocene, with the  $\delta^{18}\text{O}_{\text{diatom}}$  values recording the average  $\delta^{18}\text{O}_{\text{lakewater}}$  for  
579 summertime conditions, when the Siberian High has dissipated and increased  
580 precipitation enters the region and, thus,  $\delta^{18}\text{O}_{\text{precipitation}}$  would be relatively  
581 consistent between the Younger Dryas and Early Holocene.

582 During the Younger Dryas, southern Siberia records from lakes Baunt, Baikal  
583 and Kotokel all range between  $\sim +26$  to  $+31\text{‰}$  (Figures 6, 7 and 8). Although  
584 the resolution of the isotope record in each lake during the Younger Dryas is  
585 low (samples every  $\sim 100\text{-}600$  years), with chronological uncertainties at Lake  
586 Baunt around  $\pm 150$  years (Figures 4, 6, 7 and 8). For Baikal and Baunt  
587  $\delta^{18}\text{O}_{\text{diatom}}$  values are similar to the Mid Holocene and for Kotokel they are  
588 higher than the Holocene (Figure 8). These support our interpretation that the  
589 Baunt  $\delta^{18}\text{O}_{\text{diatom}}$  record in the Younger Dryas is influenced by the seasonality  
590 of the proxy.

591 Increased seasonality has been well documented in other proxy data from  
592 southern Siberia. Pollen evidence from both Baikal and Kotokel (Figure 6)  
593 show significant seasonality (thermal minimum summer temperatures of  
594  $\sim 12^\circ\text{C}$ , versus winter temperatures  $\sim -35^\circ\text{C}$ ) (Tarasov et al., 2007, 2009).  
595 Moreover, for Baikal, summer temperatures for the Younger Dryas show no

596 difference to the Early Holocene until the thermal maximum after ~9 ka cal BP  
597 and in Baikal only the first half of the Younger Dryas is cold in summer (Figure  
598 8). Pollen and  $\delta^{18}\text{O}_{\text{diatom}}$  records combined from Lake Baikal and Kotokel  
599 (Figure 6) suggest increasing hydrological variability due to increased  
600 precipitation from ~12.0 ka cal BP, which has been taken to indicate the region  
601 was warming (Bezrukova et al., 2010; Mackay et al., 2011; Tarasov et al.,  
602 2007, 2009). In other regions of continental Eurasia, it has been proposed that  
603 while overall conditions were cold, summers in the Younger Dryas (GS-1) were  
604 relatively warm (Schenk et al., 2018). Taking these data as a whole, we  
605 assume, that increased seasonality during the Younger Dryas may be an  
606 important influence on the Baunt  $\delta^{18}\text{O}_{\text{diatom}}$  record.

#### 607 *4.2.2. The Expression of the Early Holocene in lake Baunt and Southern* 608 *Siberia (11.7 – 8.2 ka cal BP)*

609 The Early Holocene in the Baunt record reveals considerable  $\delta^{18}\text{O}_{\text{diatom}}$   
610 variability, with peak values occurring at ~10.0 (31.0 ‰), 9.4 (31.2 ‰) and  
611 ~8.4 (32.1 ‰) ka cal BP, interrupted by lows at ~10.5 (25.9 ‰), ~9.8 (25.3 ‰),  
612 ~8.8 (25.5 ‰) and ~8.1 (26.8 ‰) ka cal BP. The amplitude of these changes,  
613 between +24‰ to +32‰ (8‰), are indicative of major hydrological variability.  
614 The higher  $\delta^{18}\text{O}_{\text{diatom}}$  values during the Early Holocene could be highlighting a  
615 response to high insolation values, and, thus, warmer temperatures (Figure  
616 7), however, higher air temperatures alone, as discussed in section 4.1, are  
617 not large enough to drive the values seen from ~10.0 ka cal BP at Baunt.

618 Previous regional studies have implicated different proportions of precipitation  
619 from some air masses to explain higher Early Holocene  $\delta^{18}\text{O}_{\text{diatom}}$  values

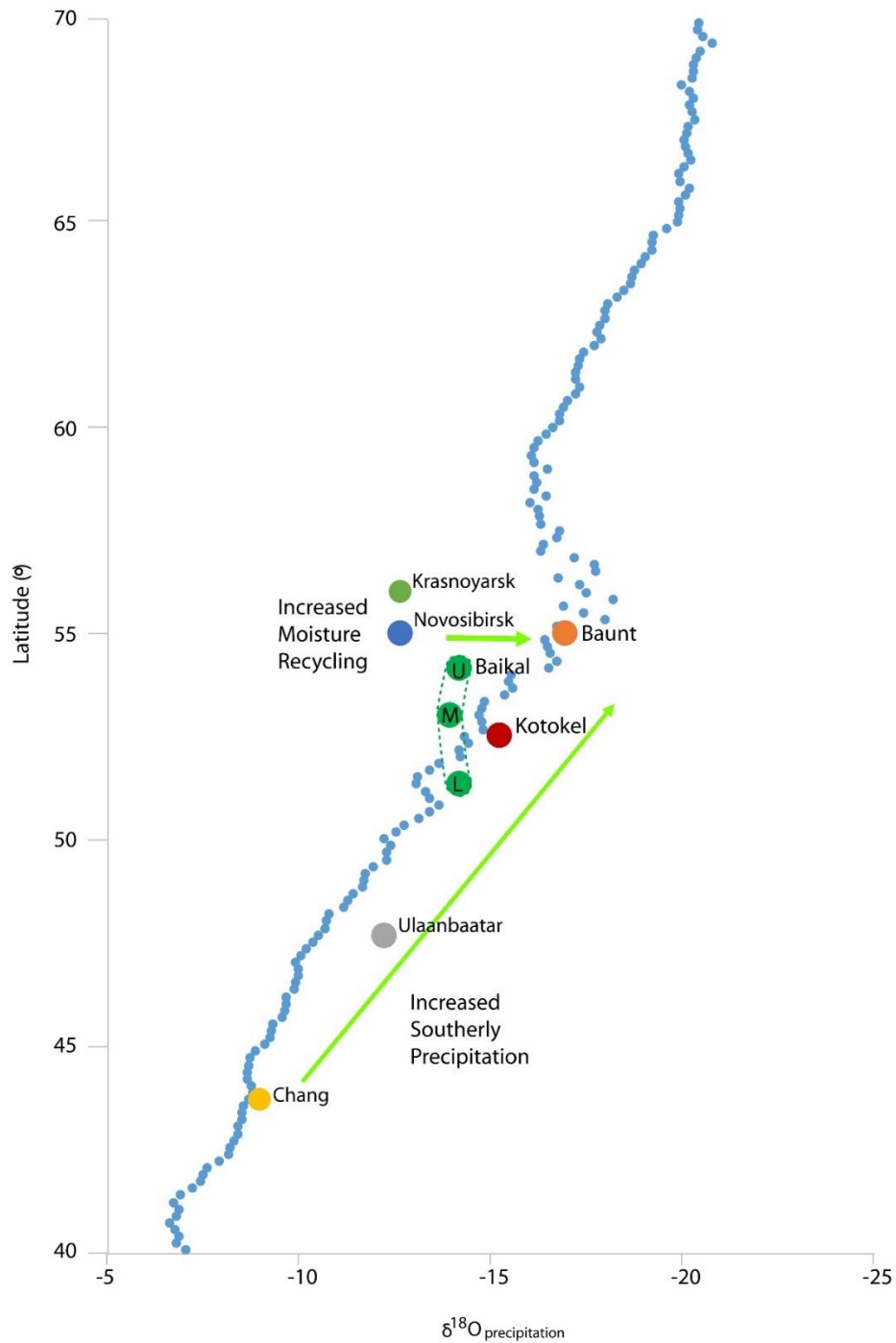


620 (Kostrova et al., 2013b, 2014, 2016). As discussed in section 1.1, the Baikal-  
621 Transbaikal region is influenced by several atmospheric circulation systems  
622 and therefore, an additional factor to consider is varying precipitation  
623 quantities and source regions. Available isotope data and models for the wider  
624 Siberian region and southern regions of Mongolia and China, from the Global  
625 Network isotopes in Precipitation (GNIP), specifically the Regionalized  
626 Cluster-Based Water Isotope Prediction (RCWIP) model (Terzer et al., 2013),  
627 allows this to be considered further (Figure 9). Currently, central and western  
628 Siberian sites have similar average  $\delta^{18}\text{O}_{\text{precipitation}}$  values (-12.6‰; Figure 9),  
629 while Lake Baunt has lower  $\delta^{18}\text{O}_{\text{precipitation}}$  by approximately 4‰ (-16.91‰).  
630 Lake Baikal's  $\delta^{18}\text{O}_{\text{precipitation}}$  is also lower than these central and western sites  
631 at ~-14‰, while Kotokel sits at -15.81‰ (Figure 9). The lower  $\delta^{18}\text{O}_{\text{precipitation}}$   
632 values at Kotokel, Baikal, and most notably Baunt, therefore, seem to be linked  
633 to the additional recycling of westerly derived moisture, and the more north  
634 eastern position of Baunt compared to Baikal and Kotokel seems to  
635 exacerbate this, while also reducing the proportion of southern sourced  
636 summertime precipitation reaching the site.

637 It is possible that weakening of the Siberian High, as a result of high solar  
638 insolation during the Early Holocene (Figure 7), allowed for increased quantity  
639 and an extended period of summertime precipitation. This resulted in increased  
640 influence of summer precipitation on the  $\delta^{18}\text{O}_{\text{lakewater}}$  values, and subsequently  
641 on the  $\delta^{18}\text{O}_{\text{diatom}}$  values. Additionally, a weaker Siberian High may have  
642 increased the proportion of southern sourced precipitation reaching the Baikal-  
643 Transbaikal region. For Lake Baunt, an increased proportion in southern  
644 sourced precipitation could induce a shift to higher  $\delta^{18}\text{O}_{\text{lakewater}}$  values and

645 consequently  $\delta^{18}\text{O}_{\text{diatom}}$  values, as  $\delta^{18}\text{O}_{\text{precipitation}}$  from southern sources are  
646 isotopically higher (Figure 9). This is shown in the  $\delta^{18}\text{O}_{\text{precipitation}}$  values from  
647 more southern sites in Mongolia and China (Figure 9), which have  
648 considerably higher (~8‰ difference) isotopic values than  $\delta^{18}\text{O}_{\text{precipitation}}$  in the  
649 Lake Baunt region, reflecting the influence of southerly sources. As modern  
650 studies (section 1.1) highlight that summertime precipitation in the Baikal-  
651 Transbaikal region currently includes a proportion of precipitation from  
652 southern sources, it is possible that increased quantities of precipitation from  
653 these sources could account for the high  $\delta^{18}\text{O}_{\text{diatom}}$  values seen in the Early  
654 Holocene.

655 A further factor that must be considered to understand the  $\delta^{18}\text{O}_{\text{diatom}}$  signal in  
656 the Early Holocene at Lake Baunt is the variation in the solar insolation  
657 received in different seasons during the Early Holocene. This is important, as  
658 the insolation received in the early summer (May-June) is substantially higher  
659 than the insolation received in mid-late summer (August-September) (Figure  
660 7). The diatom species found in the Lake Baunt record (Figure 4) are likely to  
661 be being influenced more greatly by the later summer insolation, particularly  
662 due to presence of *A. granulata*, which is often considered to bloom in the late  
663 summer during when waters have warmed and overturning occurs (Kilham  
664 and Kilham, 1975; O'Farrell et al., 2001). This species is heavily silicified and  
665 contributes substantially to the silica preserved in Baunt (Chen et al., 2012;  
666 Kilham et al., 1986), and therefore, it is likely the diatoms are again introducing  
667 a bias in the record, to mid-late summer conditions, and this could delay a  
668 record of Early Holocene warming linked to increased insolation being  
669 recorded.



671

672 **Figure 9:** Regionalized Cluster-Based Water Isotope Prediction (RCWIP)  
 673 model annual average output for  $\delta^{18}\text{O}_{\text{precipitation}}$  in 2018 (Terzer et al., 2013)  
 674 from the Global Network isotopes in Precipitation (GNIP) monitoring network.  
 675 Showing Lake Baunt (orange), Lake Kotokel (red), Lake Baikal (three green  
 676 markers for Upper, Middle and Lower basins, joined by dotted lines), plotted  
 677 against data for western central Siberian sites (blue – Novosibirsk and green  
 678 –Krasnoyarsk, Mongolian (grey – Ulaanbaatar) and a Chinese site (yellow –  
 679 Chang Chun) plotted against a transect of  $\delta^{18}\text{O}_{\text{precipitation}}$  gridded data for  $113^\circ$   
 680 longitude on a North-South latitudinal transect.

681 The occurrence of higher  $\delta^{18}\text{O}_{\text{diatom}}$  values at Lake Baunt during the Early  
682 Holocene, could, therefore, be a hydrological response to orbitally forced  
683 climate changes, leading to changes in solar insolation that then influence  
684 changes in precipitation source proportions and quantity. However, this alone  
685 cannot explain the variability seen in the  $\delta^{18}\text{O}_{\text{diatom}}$  record during this period.  
686 The Early Holocene is known to have several abrupt climate shifts  
687 superimposed over the longer term changes, and here we consider if the  
688 variability in the Baunt  $\delta^{18}\text{O}_{\text{diatom}}$  record is documenting responses to locally  
689 driven changes, or extrinsically forced shifts, with comparison with nearby  
690 lakes Baikal and Kotokel. When considering Lake Baunt alongside Lake  
691 Baikal, it is notable that both records document large amplitude  $\delta^{18}\text{O}_{\text{diatom}}$  shifts  
692 during the Early Holocene (Figures 6, 7 and 8), indicative of considerable  
693 hydrological variability (Mackay et al., 2011). Their occurrence between the  
694 two records are, however, offset, with greatest variability in Baikal occurring  
695 between  $\sim 11 - 9.5$  ka cal BP, and later at  $\sim 10.5 - 8.5$  ka cal BP at Baunt. This  
696 highlights that based on current chronological controls, peak variability occurs  
697 earlier at the more southern Lake Baikal location, possibly linked to increased  
698 regional glacier melt (Mackay et al., 2011). Mackay et al. (2011) interpret these  
699 abrupt declines in  $\delta^{18}\text{O}_{\text{diatom}}$  values in relation to ice-rafted debris evidence in  
700 North Atlantic sediments (Bond et al., 2001) indicative of slow-down of the  
701 Atlantic Meridional Overturning Circulation (AMOC) linked to fresh meltwater  
702 outbursts (Broecker, 1994).

703 In the case of Lake Baikal, the earlier onset of instability compared to Baunt  
704 could be produced by several factors. The most notable is the significant  
705 differences in catchment sizes between the two lakes, with the Lake Baikal

706 catchment extending to much more southerly latitudes than Baunt. Moreover,  
707 the Vydrino location of Lake Baikal studied by Mackay et al. (2011) is offshore  
708 from glaciers flowing into the south basin at that time. The more northerly  
709 location of glaciers affecting Lake Baunt may not have melted as rapidly or as  
710 strongly as those in regions to the south, and glaciers in the Baunt area tend  
711 to be mountain glaciers, located away from lake (Margold et al., 2016), and  
712 therefore, their influence will differ from the glaciers closely located to Baikal.  
713 The higher  $\delta^{18}\text{O}_{\text{diatom}}$  reported for the Early Holocene in Lake Baikal have been  
714 explained as being sourced through the influence of the southerly catchment  
715 from the Selenga River, contrasting with lower values through greater  
716 influence of rivers to the north (Mackay et al., 2011), coincident with reduced  
717 AMOC and increased IRD fluxes in the North Atlantic. There is a  $\sim 7\text{‰}$   
718 difference in the  $\delta^{18}\text{O}$  between these source waters (Mackay et al., 2011), and  
719 this seems to explain Baikal  $\delta^{18}\text{O}_{\text{diatom}}$  during the Early Holocene. The highest  
720  $\delta^{18}\text{O}_{\text{diatom}}$  values in Baunt are  $\sim 4\text{‰}$  lower than the highest value in Baikal,  
721 although the lowest in both are similar. Additionally to this, the complete Baunt  
722 records mean values are significantly lower than the Baikal values  
723 (supplementary information), and this indicates that the more north eastern  
724 position of Baunt and its more localised catchment, are likely to explain the  
725 lower peak values recorded in Baunt, compared to Baikal. In addition, the long  
726 residence time of water in Lake Baikal (330 years (Mackay et al., 2011)) may  
727 also be a driver of some of the discrepancies between the two lakes, as due  
728 to its smaller size and open nature, this is anticipated to be much shorter for  
729 Baunt.

730 When Lake Baunt is considered against Lake Kotokel, it is notable that  
731 variability in the Kotokel record is much more limited than that seen at Baunt  
732 (supplementary information). However, during the Early Holocene,  $\delta^{18}\text{O}_{\text{diatom}}$   
733 values at Kotokel reach levels of 29-30‰, which are only slightly (~1-2‰)  
734 lower than the peaks documented at Lake Baunt. These values at Kotokel are  
735 considered to correspond to periods of high summer insolation (Figure 7), and,  
736 as discussed above, increased proportions of precipitation from southern  
737 sources (Kostrova et al., 2013a, 2013b, 2014, 2016). This suggests both lakes  
738 are responding to the same driver, but the larger increase in values seen at  
739 Baunt are linked to its more northern position, meaning that, prior to the Early  
740 Holocene, the levels of southern precipitation reaching the site are likely to  
741 have been lower than Kotokel, and thus, an increase in lighter isotopes could  
742 cause a rapid shift in values. Slight declines in values at Kotokel during the  
743 earliest period of the Holocene have been linked to permafrost degradation  
744 and increased meltwaters (Bezrukova et al., 2010; Kostrova et al., 2016).  
745 These variations occur before shifts occur in Baunt, and this supports the  
746 findings from Baikal, suggesting that more southern sites undergo stronger  
747 glacier melting and permafrost thawing, while northern regions were later to  
748 respond. Finally, the reduced variation in the Kotokel record, compared to  
749 Baunt and Baikal, may be a result of the different characteristics of the lake,  
750 with its short residence time (7 years) (Shichi et al., 2009)(particularly  
751 compared with the long ~330 year residence time of Lake Baikal (Mackay et  
752 al., 2011)), shallower depth (Bezrukova et al., 2010; Kostrova et al., 2013b,  
753 2014, 2016) and close proximity to Baikal potentially all dampening the  
754 variability in  $\delta^{18}\text{O}_{\text{diatom}}$  record.

755 Pollen reconstructions from Kotokel and Baikal allow greater consideration of  
756 the regional landscape during this period. Both records show increasing winter  
757 temperatures, and Kotokel shows summer temperature rises, alongside  
758 annual precipitation values rising from the start of the Holocene, they do not  
759 reach peak levels until ~10.3 ka cal BP at Kotokel, and ~9.0 ka cal BP in Baikal  
760 (Tarasov et al., 2007, 2009) (Figure 6). This suggests that the earlier shifts in  
761 the Lake Baikal  $\delta^{18}\text{O}_{\text{diatom}}$  record are likely to be due to the influence of the  
762 Selenga and its southern catchment, while the Baunt signal is more likely to  
763 be representative of local conditions in its much more limited catchment.  
764 Therefore, it is also worth noting that the lag in the shift to higher  $\delta^{18}\text{O}_{\text{diatom}}$   
765 values in Baunt, by comparison to Baikal (Figures 6 and 7), may reflect not  
766 only the southerly catchment influence on Baikal, but also the more northerly  
767 position of Baunt.

768 From ~10.5 ka cal BP, Baunt begins to have evidence for large amplitude  
769 fluctuations. A decline in  $\delta^{18}\text{O}_{\text{diatom}}$  values in BNT14 at  $\sim 10.5 \pm 0.16$  may  
770 therefore appear small, but is important, as it may highlight an important shift  
771 in the regions climate, potentially showing a response to the start of regional  
772 glacial melt, as documented during the very early Holocene further south at  
773 Lake Kotokel (Bezrukova et al., 2010; Kostrova et al., 2016).

774 The large shift in the Baunt  $\delta^{18}\text{O}_{\text{diatom}}$  record at  $\sim 9.8 \pm 0.18$  ka cal BP is the most  
775 sustained during Early Holocene and occurs after the site has shown evidence  
776 of responses to increased annual temperature and precipitation during the  
777 Early Holocene, as suggested by higher  $\delta^{18}\text{O}_{\text{diatom}}$  values. A decline to lower  
778 values in Baikal at  $10.1 \pm 0.23$  overlaps with this event in Baunt, suggesting the

779 two sites may be responding to the same forcings. At Baikal this has been  
780 suggested to occur synchronously with wider northern hemisphere cooling  
781 (linked to a strong Siberian High, as indicated by peak GISP2 K+ values in  
782 Figure 7), documented in both the North Atlantic and Greenland (Bond, 1997;  
783 McManus et al., 2004; Rasmussen et al., 2014), however the timeframe of the  
784 Baunt shift does not overlap with the  $\sim 10.3$  event considered to be  
785 documented in the Baikal record. It may then be, that the records are both  
786 responding to more local forcings, or that the event in Baikal is not triggering  
787 a response to be recorded in Baunt. For Lake Baunt at this time, we consider  
788 that as previous values at  $\sim 10.0$  ka cal BP reached  $+31.0\text{‰}$ , it is likely Early  
789 Holocene warming, linked to orbital changes, triggered an increase in glacier  
790 melt local to Baunt. As  $\delta^{18}\text{O}_{\text{snowmelt}}$  is much lower than precipitation (Kostrova  
791 et al., 2020), this may be driving the decline to lower  $\delta^{18}\text{O}_{\text{diatom}}$  values. A further  
792 small decline at  $\sim 9.6 \pm 0.11$  in Baikal is not correlated to any Siberian High shifts  
793 (Figure 7) and therefore, may indicate as response to in-wash from melting  
794 glaciers, again highlighting the influence of local factors for driving changes in  
795 the  $\delta^{18}\text{O}_{\text{diatom}}$  records (Mackay et al., 2011).

796 A further decline in Baunt's  $\delta^{18}\text{O}_{\text{diatom}}$  values occurs at  $\sim 8.1 \pm 0.26$  ka cal BP,  
797 following the last of the final Early Holocene higher  $\delta^{18}\text{O}_{\text{diatom}}$  values at  
798  $8.4 \pm 0.25$ , and values continue to decline following this into the Mid Holocene.  
799 This decline is interesting, as while it coincides with the widely documented  
800 8.2 BP event, and a significant shift in Siberian High strength (Figure 7),  
801 isotopic values do not return to previous levels once the event has ended. The  
802  $\delta^{18}\text{O}_{\text{diatom}}$  record from Kotokel does not record an event at this time, while a  
803 small shift in Baikal at  $\sim 8.3 \pm 0.1$  is minor in comparison to previous fluctuations.



804 This period, however, is critical within all three records, as it marks the  
805 transition from Early Holocene into Mid Holocene hydrological conditions. All  
806 three records document a persistent shift to values below the records mean  
807 (Figure 8), while pollen reconstructions from Baikal and Kotokel show reduced  
808 precipitation from around ~8 ka cal BP (Figure 6).

809 *4.2.3. The Expression of the Mid Holocene in lake Baunt and Southern*  
810 *Siberia (~8.2 - 6.2 ka cal BP)*

811 The reduction in the amplitude of changes after ~8.2 ka cal BP in the Baunt  
812  $\delta^{18}\text{O}_{\text{diatom}}$  record may be linked to several factors, including the increased  
813 stability in the Siberian High (Figure 7) and as a result of local glaciation being  
814 limited to small mountain glaciers by this point (Margold et al., 2016), reducing  
815 the potential input of meltwaters directly into the lake. It is also possible that  
816 the Mid Holocene marks the onset of modern configuration of moisture  
817 sources to Baunt, and this appears to be supported by the greater stability in  
818 the Baikal  $\delta^{18}\text{O}_{\text{diatom}}$  values. The shift to conditions more alike those in the  
819 modern day are also supported by the pollen precipitation reconstructions,  
820 which indicate values in a range closer to the current time in Baikal and Kotokel  
821 (Tarasov et al., 2007, 2009) (Figure 6). This shift to conditions more similar to  
822 those found currently in the region may, therefore, be a driver of the greater  
823 stability documented in  $\delta^{18}\text{O}_{\text{diatom}}$  values. Alongside the stability seen in the  
824 Baunt and Baikal compared to the Early Holocene, all records show a general  
825 shift to values lower than their means across this period (Figure 8). This  
826 general decline in the  $\delta^{18}\text{O}_{\text{diatom}}$  values from the Early to the Mid Holocene  
827 supports the suggestion put forward by Kostrova et al. (2013a, 2014, 2016),

828 that during the Early Holocene a greater proportion of moisture was sourced  
829 from southern sources, causing generally higher  $\delta^{18}\text{O}_{\text{diatom}}$  values, while during  
830 the Mid Holocene, an increased amount of summertime precipitation was  
831 sourced from the Atlantic, reaching the region as recycled rainfall (Kostrova et  
832 al., 2013a, 2014, 2016) . The combined evidence from these lakes, therefore,  
833 demonstrate an important shift in the proportion of moisture from different  
834 sources between the Early to Mid Holocene. This is important, as future  
835 change within this sensitive region may bring out further changes in the  
836 proportion of moisture from different sources, altering the region's water  
837 balance.

838 In addition to the influence of changing proportions of moisture sources, the  
839 Mid Holocene also occurs as total solar insolation decreases and the relative  
840 proportion of precession increases, while obliquity declines, causing reduced  
841 seasonality (Figure 7). It is, therefore, likely that across the Mid Holocene, the  
842 record is documenting a response to changes in atmospheric circulation  
843 beyond the Siberian region, driving changes in the proportions of moisture  
844 from different source regions, alongside orbitally forced climate changes.

## 845 **5. Conclusions**

846 The Lake Baunt  $\delta^{18}\text{O}_{\text{diatom}}$  record highlights several shifts between ~13.0-6.2  
847 ka cal BP. These group into three sections, a stable early period between  
848 ~13.0-11.7 ka cal BP, a phase with large magnitude abrupt oscillations during  
849 the Early Holocene (11.7-8.2 ka cal BP) and a more muted period during the  
850 Mid Holocene (~8.2-6.2 ka cal BP), but still with some variability. These appear  
851 to reflect changes in several factors, including the source, quantity and

852 seasonality of precipitation, as well as air temperature and also long term solar  
853 insolation trends. The Younger Dryas signal at Lake Baunt is muted,  
854 potentially due to a summer season bias introduced by the diatoms, when  
855 strong seasonality driven by obliquity allows short but warm summers. During  
856 the Early Holocene higher  $\delta^{18}\text{O}_{\text{diatom}}$  values reflect the influence of high solar  
857 insolation, although this signal is delayed at Baunt, compared to more  
858 southerly records. High solar insolation induces changes in temperature and  
859 atmospheric dynamics that lead to these elevated  $\delta^{18}\text{O}_{\text{diatom}}$  values. These are  
860 punctuated by abrupt declines in  $\delta^{18}\text{O}_{\text{diatom}}$  values, which appear to be linked  
861 to local changes, particularly glacier melt. These, alongside site specific  
862 factors, notably catchment and lake size and location, explain much of the  
863 variations between the individual records from lakes in this region. This  
864 highlights the extreme sensitivity of this region, to internal variability and  
865 extrinsic forcing during times of climatic instability.

#### 866 **Acknowledgements:**

867 This work was supported by a London-NERC-DTP studentship (NERC training  
868 grant code: NE/L002485/1) and isotope analyses were funded by the National  
869 Environmental Isotope Facility (IP-1725-0517) with technical support from  
870 Hilary Sloane and Jack Lacey. Additionally, this study was performed as part  
871 of the State Research Program of IGC SB RAS IX.127.1.2 from Ministry of  
872 Education and Science of the Russian Federation, Integration Project SB RAS  
873 (grant 0341-2017-0001), RSF (grant 19-17-00216, field works), RFBR (grant  
874 20-05-00247) and Program of Government of the Russian Federation (project  
875 075-15-2019-866). Two radiocarbon dates were provided by the Quaternary

876 Research Association Chrono Award and analysed at Queens University  
877 Belfast. We thank Prof. Paula Reimer for her help with sample selection and  
878 preparation. We also thank Dr. Handong Yang (UCL) for analysis of the <sup>210</sup>Pb  
879 profile and Jim Davy for his help with SEM work.

880 **References:**

- 881 Alpat'ev, A.M., Arkhangel'skii, A.M., Podoplelov, N.Y., Stepanov, A.Y., 1976.  
882 Physical Geography of the USSR (Asiatic part). Vysshaya Shkola,  
883 Moscow.
- 884 Anchukaitis, K.J., Buckley, B.M., Cook, E.R., Cook, B.I., D'Arrigo, R.D.,  
885 Ammann, C.M., 2010. Influence of volcanic eruptions on the climate of  
886 the Asian monsoon region. *Geophys. Res. Lett.* 37, L22703.  
887 <https://doi.org/10.1029/2010GL044843>
- 888 Anekhonov, O.A., 1995. Vegetation of the Baunt Basin (Northern  
889 Transbaikalia). Novosibirsk.
- 890 Appleby, P.G., 2002. Chronostratigraphic Techniques in Recent Sediments,  
891 in: *Tracking Environmental Change Using Lake Sediments*. Kluwer  
892 Academic Publishers, Dordrecht, pp. 171–203. [https://doi.org/10.1007/0-](https://doi.org/10.1007/0-306-47669-X_9)  
893 [306-47669-X\\_9](https://doi.org/10.1007/0-306-47669-X_9)
- 894 Appleby, P.G., Nolan, P.J., Gifford, D.W., Godfrey, M.J., Oldfield, F.,  
895 Anderson, N.J., Battarbee, R.W., 1986. <sup>210</sup>Pb dating by low background  
896 gamma counting. *Hydrobiologia* 143, 21–27.  
897 <https://doi.org/10.1007/BF00026640>
- 898 Bakke, J., Lie, Ø., Heegaard, E., Dokken, T., Haug, G.H., Birks, H.H., Dulski,  
899 P., Nilsen, T., 2009. Rapid oceanic and atmospheric changes during the  
900 Younger Dryas cold period. *Nat. Geosci.* 2, 202–205.  
901 <https://doi.org/10.1038/ngeo439>
- 902 Barber, D.C., Dyke, A., Hillaire-Marcel, C., Jennings, A.E., Andrews, J.T.,  
903 Kerwin, M.W., Bilodeau, G., McNeely, R., Southon, J., Morehead, M.D.,  
904 Gagnon, J.-M., 1999. Forcing of the cold event of 8,200 years ago by  
905 catastrophic drainage of Laurentide lakes. *Nature* 400, 344–348.  
906 <https://doi.org/10.1038/22504>
- 907 Battarbee, R., Juggins, S., Gasse, F., Anderson, N., Bennion, H., Cameron,  
908 N., Ryves, D., Pailles, C., Chalif, F., Telford, R., 2001. An Information  
909 System for Palaeoenvironmental Reconstruction. *EDDI* 81, 1–94.
- 910 Bezrukova, E. V., Amosova, A.A., Chubarov, V.M., Finkelshtein, A.L.,  
911 Kulagina, N. V., 2017. Environmental changes in the northeast of the  
912 Buryat Republic during the Holocene post-Optimum: First results.  
913 *Contemp. Probl. Ecol.* 10, 431–440.  
914 <https://doi.org/10.1134/S1995425517040011>

- 915 Bezrukova, E. V., Tarasov, P.E., Solovieva, N., Krivonogov, S.K., Riedel, F.,  
916 2010. Last glacial-interglacial vegetation and environmental dynamics in  
917 southern Siberia: Chronology, forcing and feedbacks. *Palaeogeogr.*  
918 *Palaeoclimatol. Palaeoecol.* 296, 185–198.  
919 <https://doi.org/10.1016/j.palaeo.2010.07.020>
- 920 Biskaborn, B.K., Subetto, D.A., Savelieva, L.A., Vakhrameeva, P.S.,  
921 Hansche, A., Herzschuh, U., Klemm, J., Heinecke, L., Pestryakova, L.A.,  
922 Meyer, H., Kuhn, G., Diekmann, B., 2016. Late Quaternary vegetation  
923 and lake system dynamics in north-eastern Siberia: Implications for  
924 seasonal climate variability. *Quat. Sci. Rev.* 147, 406–421.  
925 <https://doi.org/10.1016/J.QUASCIREV.2015.08.014>
- 926 Blockley, S.P.E., Candy, I., Matthews, I., Langdon, P., Langdon, C., Palmer,  
927 A., Lincoln, P., Abrook, A., Taylor, B., Conneller, C., Bayliss, A.,  
928 MacLeod, A., Deepröse, L., Darvill, C., Kearney, R., Beavan, N., Staff,  
929 R., Bamforth, M., Taylor, M., Milner, N., 2018. The resilience of  
930 postglacial hunter-gatherers to abrupt climate change. *Nat. Ecol. Evol.* 2,  
931 810–818. <https://doi.org/10.1038/s41559-018-0508-4>
- 932 Blockley, S.P.E., Lane, C.S., Hardiman, M., Rasmussen, S.O., Seierstad,  
933 I.K., Steffensen, J.P., Svensson, A., Lotter, A.F., Turney, C.S.M.M.,  
934 Bronk Ramsey, C., 2012. Synchronisation of palaeoenvironmental  
935 records over the last 60,000 years, and an extended INTIMATE 1 event  
936 stratigraphy to 48,000 b2k. *Quat. Sci. Rev.* 36, 2–10.  
937 <https://doi.org/10.1016/j.quascirev.2011.09.017>
- 938 Bond, G., 1997. A Pervasive Millennial-Scale Cycle in North Atlantic  
939 Holocene and Glacial Climates. *Science* 278, 1257–1266.  
940 <https://doi.org/10.1126/science.278.5341.1257>
- 941 Bond, G., Kromer, B., Beer, J., Muscheler, R., Evans, M.N., Showers, W.,  
942 Hoffmann, S., Lotti-Bond, R., Hajdas, I., Bonani, G., 2001. Persistent  
943 solar influence on North Atlantic climate during the Holocene. *Science*  
944 294, 2130–2136. <https://doi.org/10.1126/science.1065680>
- 945 Bowen, G.J., 2020. The Online Isotopes in Precipitation Calculator [WWW  
946 Document]. version OIPC3.1 (4/2017). URL  
947 <http://www.waterisotopes.org>.
- 948 Bowen, G.J., Wassenaar, L.I., Hobson, K.A., 2005. Global application of  
949 stable hydrogen and oxygen isotopes to wildlife forensics. *Oecologia*  
950 143, 337–348. <https://doi.org/10.1007/s00442-004-1813-y>
- 951 Brauer, A., Haug, G.H., Dulski, P., Sigman, D.M., Negendank, J.F.W., 2008.  
952 An abrupt wind shift in western Europe at the onset of the Younger  
953 Dryas cold period. *Nat. Geosci.* 1, 520–523.  
954 <https://doi.org/10.1038/ngeo263>
- 955 Brewer, T.S., Leng, M.J., Mackay, A.W., Lamb, A.L., Tyler, J.J., Marsh, N.G.,  
956 2008. Unravelling contamination signals in biogenic silica oxygen  
957 isotope composition: the role of major and trace element geochemistry.  
958 *J. Quat. Sci.* 23, 321–330. <https://doi.org/10.1002/jqs.1171>

- 959 Broecker, W.S., 1994. Massive iceberg discharges as triggers for global  
960 climate change. *Nature* 372, 421–424. <https://doi.org/10.1038/372421a0>
- 961 Bronk Ramsey, C., 2009a. Dealing with outliers and offsets in radiocarbon  
962 dating. *Radiocarbon* 51, 1023–1045.  
963 <https://doi.org/https://doi.org/10.1017/S0033822200034093>
- 964 Bronk Ramsey, C., 2009b. Bayesian Analysis of Radiocarbon Dates.  
965 *Radiocarbon* 51, 337–360. [https://doi.org/10.2458/azu\\_js\\_rc.v51i1.3494](https://doi.org/10.2458/azu_js_rc.v51i1.3494)
- 966 Bronk Ramsey, C., 2008. Deposition models for chronological records. *Quat.*  
967 *Sci. Rev.* 27, 42–60.  
968 <https://doi.org/https://doi.org/10.1016/j.quascirev.2007.01.019>
- 969 Bronk Ramsey, C., Lee, S., 2013. Recent and Planned Developments of the  
970 Program OxCal. *Radiocarbon* 55, 720–730.  
971 [https://doi.org/10.2458/azu\\_js\\_rc.55.16215](https://doi.org/10.2458/azu_js_rc.55.16215)
- 972 Brooks, S.J., Matthews, I.P., Birks, H.H., Birks, H.J.B., 2012. High resolution  
973 Lateglacial and early-Holocene summer air temperature records from  
974 Scotland inferred from chironomid assemblages. *Quat. Sci. Rev.* 41, 67–  
975 82. <https://doi.org/10.1016/j.quascirev.2012.03.007>
- 976 Bush, A.B.G., 2005. CO<sub>2</sub> /H<sub>2</sub>O and orbitally driven climate variability over  
977 central Asia through the Holocene. *Quat. Int.* 136, 15–23.  
978 <https://doi.org/10.1016/j.quaint.2004.11.004>
- 979 Cartier, R., Sylvestre, F., Paillès, C., Sonzogni, C., Couapel, M., Alexandre,  
980 A., Mazur, J.C., Brisset, E., Miramont, C., Guiter, F., 2019. Diatom-  
981 oxygen isotope record from high-altitude Lake Petit (2200 m a.s.l.) in the  
982 Mediterranean Alps: Shedding light on a climatic pulse at 4.2 ka. *Clim.*  
983 *Past* 15, 253–263. <https://doi.org/10.5194/cp-15-253-2019>
- 984 Chen, X., Yang, X., Dong, X., Liu, E., 2012. Influence of environmental and  
985 spatial factors on the distribution of surface sediment diatoms in Chaohu  
986 Lake, southeast China. *Acta Bot. Croat* 71, 299–310.  
987 <https://doi.org/10.2478/v10184-011-0070-5>
- 988 Chizhova, J.N., Vasilchuk, J.Y., Yoshikawa, K., Budantseva, N.A.,  
989 Golovanov, D.L., Sorokina, O.I., Stanilovskaya, J.V., Vasil'chuk, Y.K.,  
990 2015. Isotope composition of snow cover in the Lake Baikal area. *Ice*  
991 *Snow* 55, 55–66. [https://doi.org/https://doi.org/10.15356/2076-6734-  
992 2015-3-55-66](https://doi.org/https://doi.org/10.15356/2076-6734-2015-3-55-66)
- 993 Cole-Dai, J., Ferris, D.G., Lanciki, A.L., Savarino, J., Thiemens, M.H.,  
994 McConnell, J.R., 2013. Two likely stratospheric volcanic eruptions in the  
995 1450s C.E. found in a bipolar, subannually dated 800 year ice core  
996 record. *J. Geophys. Res. Atmos.* 118, 7459–7466.  
997 <https://doi.org/10.1002/jgrd.50587>
- 998 Collins, M., Knutti, R., Arblaster, J., Dufresne, J.-L., Fichet, T.,  
999 Friedlingstein, P., Gao, X., Gutowski, W.J., Johns, T., Krinner, G.,  
1000 Shongwe, M., Tebaldi, C., Weaver, A.J., Wehner, M., 2013. Long-term  
1001 Climate Change: Projections, Commitments and Irreversibility., in:

- 1002 Stocker, T.F., Qin, D., Plattner, G.-K., Tignor, M., Allen, S.K., Boschung,  
1003 J., Nauels, A., Xia, Y., Bex, V., Midgle, P.M. (Eds.), *Climate Change*  
1004 2013: The Physical Science Basis. Contribution of Working Group I to  
1005 the Fifth Assessment Report of the Intergovernmental Panel on Climate  
1006 Change. University, Cambridge Press, Cambridge, United Kingdom and  
1007 New York, NY, USA.
- 1008 Coope, G.R., Lemdahl, G., Lowe, J.J., Walkling, A., 1998. Temperature  
1009 gradients in northern Europe during the last glacial–Holocene transition  
1010 (14–9 14C kyr BP) interpreted from coleopteran assemblages. *J. Quat.*  
1011 *Sci.* 13, 419–433. [https://doi.org/10.1002/\(SICI\)1099-](https://doi.org/10.1002/(SICI)1099-1417(199809)13:5<419::AID-JQS410>3.0.CO;2-D)  
1012 [1417\(199809\)13:5<419::AID-JQS410>3.0.CO;2-D](https://doi.org/10.1002/(SICI)1099-1417(199809)13:5<419::AID-JQS410>3.0.CO;2-D)
- 1013 Deluca, T.H., Boisvenue, C., 2012. Boreal forest soil carbon: distribution,  
1014 function and modelling. *For. An Int. J. For. Res.* 85, 161–184.  
1015 <https://doi.org/10.1093/forestry/cps003>
- 1016 Dodd, J.P., Sharp, Z.D., 2010. A laser fluorination method for oxygen isotope  
1017 analysis of biogenic silica and a new oxygen isotope calibration of  
1018 modern diatoms in freshwater environments. *Geochim. Cosmochim.*  
1019 *Acta* 74, 1381–1390. <https://doi.org/10.1016/j.gca.2009.11.023>
- 1020 Dong, J., Wang, Y., Cheng, H., Hardt, B., Edwards, R.L., Xinggong Kong, X.,  
1021 Jiangying Wu, J., Shitao Chen, S., Dianbing Liu, D., Xiuyang Jiang, X.,  
1022 Kan Zhao, K., 2010. A high-resolution stalagmite record of the Holocene  
1023 East Asian monsoon from Mt Shennongjia, central China. *The Holocene*  
1024 20, 257–264. <https://doi.org/10.1177/0959683609350393>
- 1025 Dykoski, C.A., Edwards, R.L., Cheng, H., Yuan, D., Cai, Y., Zhang, M., Lin,  
1026 Y., Qing, J., An, Z., Revenaugh, J., Dykoski, C.A., Edwards, R.L.,  
1027 Cheng, H., Yuan, D., Cai, Y., Zhang, M., Lin, Y., Qing, J., An, Z.,  
1028 Revenaugh, J., Dykosko, C., Edwards, R.L., Cheng, H., Yuan, D., Cai,  
1029 Y., Zhang, M., Lin, Y., Qing, J., An, Z., Revenaugh, J., 2005. A high-  
1030 resolution, absolute-dated Holocene and deglacial Asian monsoon  
1031 record from Dongge Cave, China. *Earth Planet. Sci. Lett.* 233, 71–86.  
1032 <https://doi.org/10.1016/j.epsl.2005.01.036>
- 1033 Fletcher, W.J., Sánchez Goñi, M.F., Allen, J.R.M., Cheddadi, R.,  
1034 Combourieu-Nebout, N., Huntley, B., Lawson, I., Londeix, L., Magri, D.,  
1035 Margari, V., Müller, U.C., Naughton, F., Novenko, E., Roucoux, K.,  
1036 Tzedakis, P.C., 2010. Millennial-scale variability during the last glacial in  
1037 vegetation records from Europe. *Quat. Sci. Rev.* 29, 2839–2864.  
1038 <https://doi.org/10.1016/J.QUASCIREV.2009.11.015>
- 1039 Flower, R., Ryves, D., 2009. Diatom preservation: differential preservation of  
1040 sedimentary diatoms in two saline lakes. *Acta Bot. Croat.* 68, 381–399.
- 1041 Heiri, O., Millet, L., 2005. Reconstruction of Late Glacial summer  
1042 temperatures from chironomid assemblages in Lac Lautrey (Jura,  
1043 France). *J. Quat. Sci.* 20, 33–44. <https://doi.org/10.1002/jqs.895>
- 1044 Heiri, O., Tinner, W., Lotter, A.F., 2004. Evidence for cooler European  
1045 summers during periods of changing meltwater flux to the North Atlantic.

- 1046 Proc. Natl. Acad. Sci. U. S. A. 101, 15285–15288.  
1047 <https://doi.org/10.1073/pnas.0406594101>
- 1048 Hoek, W.Z., Bos, J.A.A., 2007. Early Holocene climate oscillations—causes  
1049 and consequences. *Quat. Sci. Rev.* 26, 1901–1906.  
1050 <https://doi.org/10.1016/j.quascirev.2007.06.008>
- 1051 Huhne, C., Slingo, J. (eds), 2011. *Climate: Observations, projections and*  
1052 *impacts - Russia*, Met Office Publication.
- 1053 Jansen, E., Overpeck, J., Briffa, K.R., Duplessy, J.-C., Joos, F., Masson-  
1054 Delmotte, V., Olago, D., Otto-Bliesner, B., Richard Peltier, W.,  
1055 Rahmstorf, S., Ramesh, R., Raynaud, D., Rind, D., Solomina, O.,  
1056 Villalba, R., Zhang, D., 2007. Palaeoclimate: 6.5.1 Climate Forcing and  
1057 Response During the Current Interglacial, in: Solomon, S., Qin, D.,  
1058 Manning, M., Chen, Z., Marquis, M., Averyt, K.B., Tignor, M., Miller, H.L.  
1059 (Ed.), *Climate Change 2007: The Physical Science Basis. Contribution*  
1060 *of Working Group I to the Fourth Assessment Report of the*  
1061 *Intergovernmental Panel on Climate Change*. Cambridge University  
1062 Press, Cambridge, UK and New York, NY, USA, pp. 459–462.
- 1063 Juggins, S., 2016. C2 Data Analysis. Network Version 1.7.7 Beta University  
1064 of Newcastle, Newcastle (2004).
- 1065 Katsuta, N., Ikeda, H., Shibata, K., Saito-Kokubu, Y., Murakami, T., Tani, Y.,  
1066 Takano, M., Nakamura, T., Tanaka, A., Naito, S., Ochiai, S., Shichi, K.,  
1067 Kawakami, S., Kawai, T., 2018. Hydrological and climate changes in  
1068 southeast Siberia over the last 33 kyr. *Glob. Planet. Change* 164, 11–26.  
1069 <https://doi.org/10.1016/j.gloplacha.2018.02.012>
- 1070 Kilham, P., Kilham, S.S., Hecky, R.E., 1986. Hypothesized resource  
1071 relationships among African planktonic diatoms. *Limnol. Oceanogr.* 31,  
1072 1169–1181. <https://doi.org/10.4319/lo.1986.31.6.1169>
- 1073 Kilham, S.S., Kilham, P., 1975. *Melosira granulata* (Ehr.) Ralfs: morphology  
1074 and ecology of a cosmopolitan freshwater diatom. *SIL Proceedings*,  
1075 1922-2010 19, 2716–2721.  
1076 <https://doi.org/10.1080/03680770.1974.11896368>
- 1077 Kingston, J.D., 2005. Orbital controls on seasonality, in: Brockman, D.K., van  
1078 Schaik, C.P. (Eds.), *Seasonality in Primates: Studies of Living and*  
1079 *Extinct Human and Non-Human Primates*. Cambridge University Press,  
1080 Cambridge, pp. 520–541.
- 1081 Kostrova, S. S., Meyer, H., Bailey, H.L., Ludikova, A. V., Gromig, R., Kuhn,  
1082 G., Shibaev, Y.A., Kozachek, A. V., Ekaykin, A.A., Chaplign, B., 2019.  
1083 Holocene hydrological variability of Lake Ladoga, northwest Russia, as  
1084 inferred from diatom oxygen isotopes. *Boreas* 48, 361–376.  
1085 <https://doi.org/10.1111/bor.12385>
- 1086 Kostrova, S. S., Meyer, H., Chaplign, B., Bezrukova, E. V., Tarasov, P.E.,  
1087 Kuz'min, M.I., 2013a. Reconstruction of the Holocene climate of  
1088 Transbaikalia: Evidence from the oxygen isotope analysis of fossil



- 1089 diatoms from Kotokel Lake. *Dokl. Earth Sci.* 451, 732–736.  
1090 <https://doi.org/10.1134/S1028334X13070039>
- 1091 Kostrova, S. S., Meyer, H., Chapligin, B., Kossler, A., Bezrukova, E. V.,  
1092 Tarasov, P.E., 2013b. Holocene oxygen isotope record of diatoms from  
1093 Lake Kotokel (southern Siberia, Russia) and its palaeoclimatic  
1094 implications. *Quat. Int.* 290–291, 21–34.  
1095 <https://doi.org/10.1016/j.quaint.2012.05.011>
- 1096 Kostrova, S. S., Meyer, H., Chapligin, B., Tarasov, P.E., Bezrukova, E. V.,  
1097 2014. The last glacial maximum and late glacial environmental and  
1098 climate dynamics in the Baikal region inferred from an oxygen isotope  
1099 record of lacustrine diatom silica. *Quat. Int.* 348, 25–36.  
1100 <https://doi.org/10.1016/j.quaint.2014.07.034>
- 1101 Kostrova, S. S., Meyer, H., Fernandoy, F., Werner, M., Tarasov, P.E., 2020.  
1102 Moisture origin and stable isotope characteristics of precipitation in  
1103 southeast Siberia. *Hydrol. Process.* 34, 51–67.  
1104 <https://doi.org/10.1002/hyp.13571>
- 1105 Kostrova, S. S., Meyer, H., Tarasov, P.E., Bezrukova, E. V., Chapligin, B.,  
1106 Kossler, A., Pavlova, L.A., Kuzmin, M.I., 2016. Oxygen isotope  
1107 composition of diatoms from sediments of Lake Kotokel (Buryatia).  
1108 *Russ. Geol. Geophys.* 57, 1239–1247.  
1109 <https://doi.org/10.1016/j.rgg.2016.08.009>
- 1110 Kozhov, M.M., 1950. Fresh water of Eastern Siberia. OGIZ Press, Irkutsk.
- 1111 Krainov, M.A., Bezrukova, E. V., Shchetnikov, A.A., Kerber, E. V., 2018. First  
1112 Data on the Gothenburg and Mono Lake Excursions in Paleomagnetic  
1113 Records from Bottom Sediments of Lakes of Transbaikalia (Exemplified  
1114 by Baunt Lake). *Dokl. Earth Sci.* 481, 980–983.  
1115 <https://doi.org/10.1134/S1028334X18080068>
- 1116 Krainov, M.A., Bezrukova, E. V., Kerber, E. V., Levina, O. V., Ivanov, E. V.,  
1117 Shchetnikov, A.A., Filinov, I.A., 2017. First results of study of Lake Baunt  
1118 bottom sediments (northern Transbaikalia). *Russ. Geol. Geophys.* 58,  
1119 1401–1411. <https://doi.org/10.1016/j.rgg.2017.02.005>
- 1120 Lane, C.S., Brauer, A., Blockley, S.P.E., Dulski, P., 2013. Volcanic ash  
1121 reveals time-transgressive abrupt climate change during the Younger  
1122 Dryas. *Geology* 41, 1251–1254. <https://doi.org/10.1130/G34867.1>
- 1123 Laskar, J., Robutel, P., Joutel, F., Gastineau, M., Correia, A.C.M.M., Levrard,  
1124 B., 2004. A long-term numerical solution for the insolation quantities of  
1125 the Earth. *Astron. Astrophys.* 428, 261–285.  
1126 <https://doi.org/10.1051/0004-6361:20041335>
- 1127 Leemans, R., Cramer, W.P., 1991. The IIASA Database for Mean Monthly  
1128 Values of Temperature , Precipitation , and Cloudiness on a Global  
1129 Terrestrial Grid, Environmental Protection. RR-91-018.
- 1130 Leng, M.J., Barker, P.A., 2006. A review of the oxygen isotope composition  
1131 of lacustrine diatom silica for palaeoclimate reconstruction. *Earth-*

- 1132 Science Rev. 75, 5–27.  
1133 <https://doi.org/https://doi.org/10.1016/j.earscirev.2005.10.001>
- 1134 Leng, M.J., Marshall, J.D., 2004. Palaeoclimate interpretation of stable  
1135 isotope data from lake sediment archives. *Quat. Sci. Rev.* 23, 811–831.  
1136 <https://doi.org/10.1016/j.quascirev.2003.06.012>
- 1137 Leng, M.J., Sloane, H.J., 2008. Combined oxygen and silicon isotope  
1138 analysis of biogenic silica. *J. Quat. Sci.* 23, 313–319.  
1139 <https://doi.org/10.1002/jqs.1177>
- 1140 Leng, M.J., Swann, G.E.A., 2010. Stable Isotopes from Diatom Silica, in:  
1141 Smol, J.P.; Stoermer, E.F. (Ed.), *The Diatoms : Applications for the*  
1142 *Environmental and Earth Sciences*. Cambridge University Press,  
1143 Cambridge, pp. 127–143.
- 1144 Lisiecki, L.E., Raymo, M.E., 2005. A Pliocene-Pleistocene stack of 57  
1145 globally distributed benthic  $\delta^{18}\text{O}$  records. *Paleoceanography* 20,  
1146 PA1003 (1-17). <https://doi.org/10.1029/2004PA001071>
- 1147 Liu, Z., Zhu, J., Rosenthal, Y., Zhang, X., Otto-Bliesner, B.L., Timmermann,  
1148 A., Smith, R.S., Lohmann, G., Zheng, W., Elison Timm, O., 2014. The  
1149 Holocene temperature conundrum. *Proc. Natl. Acad. Sci. U. S. A.* 111,  
1150 E3501-5. <https://doi.org/10.1073/pnas.1407229111>
- 1151 Lowe, J.J., Walker, M.J.C., 2015. *Reconstructing Quaternary Environments*,  
1152 3rd ed. Routledge, London and New York.
- 1153 Mackay, A.W., Bezrukova, E. V., Boyle, J.F., Holmes, J.A., Panizzo, V.N.,  
1154 Piotrowska, N., Shchetnikov, A., Shilland, E.M., Tarasov, P., White, D.,  
1155 2013a. Multiproxy evidence for abrupt climate change impacts on  
1156 terrestrial and freshwater ecosystems in the Ol'khon region of Lake  
1157 Baikal, central Asia. *Quat. Int.* 290–291, 46–56.  
1158 <https://doi.org/10.1016/j.quaint.2012.09.031>
- 1159 Mackay, A.W., Ryves, D.B., Battarbee, R.W., Flower, R.J., Jewson, D.,  
1160 Rioual, P., Sturm, M., 2005. 1000 years of climate variability in central  
1161 Asia: assessing the evidence using Lake Baikal (Russia) diatom  
1162 assemblages and the application of a diatom-inferred model of snow  
1163 cover on the lake. *Glob. Planet. Change* 46, 281–297.  
1164 <https://doi.org/10.1016/j.gloplacha.2004.09.021>
- 1165 Mackay, A.W., Swann, G.E. a., Fagel, N., Fietz, S., Morley, D., Rioual, P.,  
1166 Tarasov, P., Leng, M.J., 2013b. Hydrological instability during the Last  
1167 Interglacial in central Asia: a new diatom oxygen isotope record from  
1168 Lake Baikal. *Quat. Sci. Rev.* 66, 45–54.  
1169 <https://doi.org/10.1016/j.quascirev.2012.09.025>
- 1170 Mackay, A.W., Swann, G.E.A., Brewer, T.S., Leng, M.J., Morley, D.W.,  
1171 Piotrowska, N., Rioual, P., White, D., 2011. A reassessment of late  
1172 glacial - Holocene diatom oxygen isotope record from Lake Baikal using  
1173 a geochemical mass-balance approach. *J. Quat. Sci.* 26, 627–634.  
1174 <https://doi.org/10.1002/jqs.1484>

- 1175 Margold, M., Jansen, J.D., Gurinov, A.L., Codilean, A.T., Fink, D., Preusser,  
1176 F., Reznichenko, N. V., Mifsud, C., 2016. Extensive glaciation in  
1177 Transbaikalia, Siberia, at the Last Glacial Maximum. *Quat. Sci. Rev.*  
1178 132, 161–174. <https://doi.org/10.1016/j.quascirev.2015.11.018>
- 1179 Martin, M., Jansson, K.N., 2011. Glacial geomorphology and glacial lakes of  
1180 central Transbaikalia, Siberia, Russia. *J. Maps* 7, 18–30.  
1181 <https://doi.org/10.4113/jom.2011.1132>
- 1182 Mayewski, P.A., Rohling, E.E., Curt Stager, J., Karlén, W., Maasch, K.A.,  
1183 David Meeker, L., Meyerson, E.A., Gasse, F., van Kreveld, S.,  
1184 Holmgren, K., Lee-Thorp, J., Rosqvist, G., Rack, F., Staubwasser, M.,  
1185 Schneider, R.R., Steig, E.J., 2004. Holocene climate variability. *Quat.*  
1186 *Res.* 62, 243–255. <https://doi.org/10.1016/J.YQRES.2004.07.001>
- 1187 McManus, J.F., Francois, R., Gherardi, J.-M., Keigwin, L.D., Brown-Leger,  
1188 S., 2004. Collapse and rapid resumption of Atlantic meridional  
1189 circulation linked to deglacial climate changes. *Nature* 428, 834–837.  
1190 <https://doi.org/10.1038/nature02494>
- 1191 Meyer, H., Chaplignin, B., Hoff, U., Nazarova, L., Diekmann, B., 2015. Oxygen  
1192 isotope composition of diatoms as Late Holocene climate proxy at Two-  
1193 Yurts Lake, Central Kamchatka, Russia. *Glob. Planet. Change* 134,  
1194 118–128. <https://doi.org/10.1016/j.gloplacha.2014.04.008>
- 1195 Meyer, H., Schönicke, L., Wand, U., Hubberten, H.W., Friedrichsen, H.,  
1196 2000. Isotope Studies of Hydrogen and Oxygen in Ground Ice -  
1197 Experiences with the Equilibration Technique. *Isotopes Environ. Health*  
1198 *Stud.* 36, 133–149. <https://doi.org/10.1080/10256010008032939>
- 1199 Moore, M. V., Hampton, S.E., Izmet'eva, L.R., Silow, E.A., Peshkova, E. V.,  
1200 Pavlov, B.K., 2009. Climate Change and the World's "Sacred Sea"—  
1201 Lake Baikal, Siberia. *Bioscience* 59, 405–417.  
1202 <https://doi.org/10.1525/bio.2009.59.5.8>
- 1203 Morley, D.W., Leng, M.J., Mackay, A.W., Sloane, H.J., 2005. Late glacial and  
1204 Holocene environmental change in the Lake Baikal region documented  
1205 by oxygen isotopes from diatom silica. *Glob. Planet. Change* 46, 221–  
1206 233. <https://doi.org/10.1016/j.gloplacha.2004.09.018>
- 1207 Morley, D.W., Leng, M.J., Mackay, A.W., Sloane, H.J., Rioual, P., Battarbee,  
1208 R.W., 2004. Cleaning of lake sediment samples for diatom oxygen  
1209 isotope analysis. *J. Paleolimnol.* 31, 391–401.  
1210 <https://doi.org/10.1023/B:JOPL.0000021854.70714.6b>
- 1211 Müller, S., Tarasov, P.E., Hoelzmann, P., Bezrukova, E. V., Kossler, A.,  
1212 Krivonogov, S.K., 2014. Stable vegetation and environmental conditions  
1213 during the Last Glacial Maximum: New results from Lake Kotokel (Lake  
1214 Baikal region, southern Siberia, Russia). *Quat. Int.* 348, 14–24.  
1215 <https://doi.org/10.1016/J.QUAINT.2013.12.012>
- 1216 Nenakhov, V.M., Nikitin, A. V., 2007. Structure, magmatism, and Paleozoic  
1217 tectonic evolution of the Uakit Zone in the context of the formation of the

- 1218 Angara-Vitim batholith in the western Transbaikal region. *Geotectonics*  
1219 41, 114–129. <https://doi.org/10.1134/S0016852107020033>
- 1220 O'Farrell, I., Tell, G., Podlejski, A., 2001. Morphological variability of  
1221 *Aulacoseira granulata* (Ehr.) Simonsen (Bacillariophyceae) in the Lower  
1222 Parana River (Argentina). *Limnology* 2, 65–71.  
1223 <https://doi.org/10.1007/s102010170001>
- 1224 Osipova, O.P., Osipov, E.Y., 2019. Atmospheric Circulation Processes and  
1225 Precipitation Regime in the Northern Part of the Baikal Mountain Region.  
1226 *Russ. Meteorol. Hydrol.* 44, 695–703.  
1227 <https://doi.org/10.3103/S106837391910008X>
- 1228 Park, T.-W., Jeong, J.-H., Deng, Y., Zhou, R., Cai, M., 2014. Quantitative  
1229 decomposition of radiative and non-radiative contributions to  
1230 temperature anomalies related to siberian high variability. *Clim. Dyn.* 45,  
1231 1207–1217. <https://doi.org/10.1007/s00382-014-2371-6>
- 1232 Pavlova, L.A., Tkachenko, L.L., Goreglyad, A.V., Kuzmin, M.I., 2014.  
1233 Peculiarities Of The Diatom Valve Chemical Composition (Inorganic  
1234 Components) Study By Electron Probe X-Ray Microanalysis. *Methods*  
1235 *Objects Chem. Anal.* 9, 65–72. [https://doi.org/10.17721/moca.2014.65-](https://doi.org/10.17721/moca.2014.65-72)  
1236 [72](https://doi.org/10.17721/moca.2014.65-72)
- 1237 Prokopenko, A.A., Williams, D.F., 2004. Deglacial methane emission signals  
1238 in the carbon isotopic record of Lake Baikal. *Earth Planet. Sci. Lett.* 218,  
1239 135–147. [https://doi.org/10.1016/S0012-821X\(03\)00637-X](https://doi.org/10.1016/S0012-821X(03)00637-X)
- 1240 Prokopenko, A.A., Williams, D.F., Karabanov, E.B., Khursevich, G.K., 1999.  
1241 Response of Lake Baikal ecosystem to climate forcing and pCO<sub>2</sub>  
1242 change over the last glacial/interglacial transition. *Earth Planet. Sci. Lett.*  
1243 172, 239–253. [https://doi.org/10.1016/S0012-821X\(99\)00203-4](https://doi.org/10.1016/S0012-821X(99)00203-4)
- 1244 Prokopenko, A.A., Williams, D.F., Kuzmin, M.I., Karabanov, E.B.,  
1245 Khursevich, G.K., Peck, J.A., 2002. Muted climate variations in  
1246 continental Siberia during the mid-Pleistocene epoch. *Nature* 418, 65–  
1247 68. <https://doi.org/10.1038/nature00886>
- 1248 Rach, O., Brauer, A., Wilkes, H., Sachse, D., 2014. Delayed hydrological  
1249 response to Greenland cooling at the onset of the Younger Dryas in  
1250 western Europe. *Nat. Geosci.* 7, 109–112.  
1251 <https://doi.org/10.1038/ngeo2053>
- 1252 Rasmussen, S.O., Bigler, M., Blockley, S.P.E., Blunier, T., Buchardt, S.L.,  
1253 Clausen, H.B., Cvijanovic, I., Dahl-Jensen, D., Johnsen, S.J., Fischer,  
1254 H., Gkinis, V., Guillevic, M., Hoek, W.Z., Lowe, J.J., Pedro, J.B., Popp,  
1255 T., Seierstad, I.K., Steffensen, J.P., Svensson, A.M., Vallelonga, P.,  
1256 Vinther, B.M., Walker, M.J.C., Wheatley, J.J., Winstrup, M., 2014. A  
1257 stratigraphic framework for abrupt climatic changes during the Last  
1258 Glacial period based on three synchronized Greenland ice-core records:  
1259 Refining and extending the INTIMATE event stratigraphy. *Quat. Sci.*  
1260 *Rev.* 106, 14–28. <https://doi.org/10.1016/j.quascirev.2014.09.007>

- 1261 Reed, S.J.B.B., 2005. Electron Microprobe Analysis and Scanning Electron  
1262 Microscopy in Geology, Electron Microprobe Analysis and Scanning  
1263 Electron Microscopy in Geology. Cambridge University Press.  
1264 <https://doi.org/10.1017/CBO9780511610561>
- 1265 Reimer, P., Baillie, M., Bard, E., 2009. IntCal09 and Marine09 radiocarbon  
1266 age calibration curves, 0-50,000 years cal BP. *Radiocarbon* 51, 1111–  
1267 1150.
- 1268 Reimer, P.J., Austin, W.E.N., Bard, E., Bayliss, A., Blackwell, P.G., Bronk  
1269 Ramsey, C., Butzin, M., Cheng, H., Edwards, R.L., Friedrich, M.,  
1270 Grootes, P.M., Guilderson, T.P., Hajdas, I., Heaton, T.J., Hogg, A.G.,  
1271 Hughen, K.A., Kromer, B., Manning, S.W., Muscheler, R., Palmer, J.G.,  
1272 Pearson, C., van der Plicht, J., Reimer, R.W., Richards, D.A., Scott,  
1273 E.M., Southon, J.R., Turney, C.S.M., Wacker, L., Adolphi, F., Büntgen,  
1274 U., Capano, M., Fahrni, S.M., Fogtmann-Schulz, A., Friedrich, R.,  
1275 Köhler, P., Kudsk, S., Miyake, F., Olsen, J., Reinig, F., Sakamoto, M.,  
1276 Sookdeo, A., Talamo, S., 2020. The IntCal20 Northern Hemisphere  
1277 Radiocarbon Age Calibration Curve (0-55 cal kBP). *Radiocarbon* 00, 1–  
1278 33. <https://doi.org/10.1017/rdc.2020.41>
- 1279 Renssen, H., Seppä, H., Crosta, X., Goosse, H., Roche, D.M., 2012. Global  
1280 characterization of the Holocene Thermal Maximum. *Quat. Sci. Rev.* 48,  
1281 7–19. <https://doi.org/10.1016/J.QUASCIREV.2012.05.022>
- 1282 Rioual, P., Mackay, A.W., 2005. A diatom record of centennial resolution for  
1283 the Kazantsevo Interglacial stage in Lake Baikal (Siberia). *Glob. Planet.*  
1284 *Change* 46, 199–219. <https://doi.org/10.1016/j.gloplacha.2004.08.002>
- 1285 Rohling, E.J., Pälike, H., 2005. Centennial-scale climate cooling with a  
1286 sudden cold event around 8,200 years ago. *Nature* 434, 975–979.  
1287 <https://doi.org/10.1038/nature03421>
- 1288 Romanovsky, V.E., Drozdov, D.S., Oberman, N.G., Malkova, G. V.,  
1289 Kholodov, A.L., Marchenko, S.S., Moskalenko, N.G., Sergeev, D.O.,  
1290 Ukraintseva, N.G., Abramov, A.A., Gilichinsky, D.A., Vasiliev, A.A.,  
1291 2010. Thermal state of permafrost in Russia. *Permafr. Periglac.*  
1292 *Process.* 21, 136–155. <https://doi.org/10.1002/ppp.683>
- 1293 Ryabenko, V.E., Sidorenko, A.B., Florensov, N.A., 1964. Geology of the  
1294 USSR. V. xxxv. Buryat Autonomous Soviet Socialist Republic. Part 1.  
1295 Geological description, 5. 35. ed. Nedra, - M.:
- 1296 Rytsk, E.Y., Kovach, V.P., Kovalenko, V.I., Yarmolyuk, V. V., 2007. Structure  
1297 and evolution of the continental crust in the Baikal Fold Region.  
1298 *Geotectonics* 41, 440–464. <https://doi.org/10.1134/S0016852107060027>
- 1299 Ryves, D., Juggins, S., Fritz, S., Battarbee, R., 2001. Experimental diatom  
1300 dissolution and the quantification of microfossil preservation in  
1301 sediments. *Palaeogeogr. Palaeoclimatol. Palaeoecol.* 172, 99–113.  
1302 [https://doi.org/10.1016/S0031-0182\(01\)00273-5](https://doi.org/10.1016/S0031-0182(01)00273-5)
- 1303 Schenk, F., Väiliranta, M., Muschitiello, F., Tarasov, L., Heikkilä, M., Björck,

- 1304 S., Brandefelt, J., Johansson, A. V., Näslund, J.-O., Wohlfarth, B., 2018.  
 1305 Warm summers during the Younger Dryas cold reversal. *Nat. Commun.*  
 1306 9, 1634. <https://doi.org/10.1038/s41467-018-04071-5>
- 1307 Schlolaut, G., Brauer, A., Nakagawa, T., Lamb, H.F., Tyler, J.J., Staff, R.A.,  
 1308 Marshall, M.H., Bronk Ramsey, C., Bryant, C.L., Tarasov, P.E., 2017.  
 1309 Evidence for a bi-partition of the Younger Dryas Stadial in East Asia  
 1310 associated with inversed climate characteristics compared to Europe.  
 1311 *Sci. Rep.* 7, 44983. <https://doi.org/10.1038/srep44983>
- 1312 Shchetnikov, A.A., 2007. Morphotectonics of lacustrine basins: The Baikal rift  
 1313 zone as an example. *Russ. J. Pacific Geol.* 1, 120–129.  
 1314 <https://doi.org/10.1134/S1819714007020029>
- 1315 Shichi, K., Takahara, H., Krivonogov, S.K., Bezrukova, E. V., Kashiwaya, K.,  
 1316 Takehara, A., Nakamura, T., 2009. Late Pleistocene and Holocene  
 1317 vegetation and climate records from Lake Kotokel, central Baikal region.  
 1318 *Quat. Int.* 205, 98–110. <https://doi.org/10.1016/j.quaint.2009.02.005>
- 1319 Sigl, M., Winstrup, M., McConnell, J.R., Welten, K.C., Plunkett, G., Ludlow,  
 1320 F., Büntgen, U., Caffee, M., Chellman, N., Dahl-Jensen, D., Fischer, H.,  
 1321 Kipfstuhl, S., Kostick, C., Maselli, O.J., Mekhaldi, F., Mulvaney, R.,  
 1322 Muscheler, R., Pasteris, D.R., Pilcher, J.R., Salzer, M., Schüpbach, S.,  
 1323 Steffensen, J.P., Vinther, B.M., Woodruff, T.E., 2015. Timing and climate  
 1324 forcing of volcanic eruptions for the past 2,500 years. *Nature* 523, 543–  
 1325 549. <https://doi.org/10.1038/nature14565>
- 1326 Smith, A.C., Leng, M.J., Swann, G.E.A., Barker, P.A., Mackay, A.W., Ryves,  
 1327 D.B., Sloane, H.J., Chenery, S.R.N., Hems, M., 2016. An experiment to  
 1328 assess the effects of diatom dissolution on oxygen isotope ratios. *Rapid*  
 1329 *Commun. Mass Spectrom.* 30, 293–300.  
 1330 <https://doi.org/10.1002/rcm.7446>
- 1331 Solotchin, P.A., Sklyarov, E. V., Solotchina, E.P., Zamana, L. V., Sklyarova,  
 1332 O.A., Solotchin, P. A., Sklyarov, E. V., Solotchina, E. P., Zamana, L. V.,  
 1333 Sklyarova, O.A., 2015. A New Find of Kogarkoite Na<sub>3</sub>SO<sub>4</sub>F in  
 1334 Transbaikalia. *Dokl. Earth Sci.* 462, 643–647.  
 1335 <https://doi.org/10.1134/S1028334X15060239>
- 1336 Stebich, M., Mingram, J., Han, J., Liu, J., 2009. Late Pleistocene spread of  
 1337 (cool-)temperate forests in Northeast China and climate changes  
 1338 synchronous with the North Atlantic region. *Glob. Planet. Change* 65,  
 1339 56–70. <https://doi.org/https://doi.org/10.1016/j.gloplacha.2008.10.010>
- 1340 Steffensen, J.P., Andersen, K.K., Bigler, M., Clausen, H.B., Dahl-Jensen, D.,  
 1341 Fischer, H., Goto-Azuma, K., Hansson, M., Johnsen, S.J., Jouzel, J.,  
 1342 Masson-Delmotte, V., Popp, T., Rasmussen, S.O., Röthlisberger, R.,  
 1343 Ruth, U., Stauffer, B., Siggaard-Andersen, M.-L., Sveinbjörnsdóttir, Á.E.,  
 1344 Svensson, A., White, J.W.C., Sveinbjörnsdóttir, A.E., Svensson, A.,  
 1345 White, J.W.C., 2008. High-resolution Greenland ice core data show  
 1346 abrupt climate change happens in few years. *Science* 321, 680–684.  
 1347 <https://doi.org/10.1126/science.1157707>

- 1348 Stokes, C.R., Shahgedanova, M., Evans, I.S., Popovnin, V. V., 2013.  
1349 Accelerated loss of alpine glaciers in the Kodar Mountains, south-  
1350 eastern Siberia. *Glob. Planet. Change* 101, 82–96.  
1351 <https://doi.org/10.1016/j.gloplacha.2012.12.010>
- 1352 Swann, G.E.A., Leng, M.J., 2009. A review of diatom  $\delta^{18}\text{O}$  in  
1353 palaeoceanography. *Quat. Sci. Rev.* 28, 384–398.  
1354 <https://doi.org/10.1016/j.quascirev.2008.11.002>
- 1355 Swann, G.E.A., Leng, M.J., Juschus, O., Melles, M., Brigham-Grette, J.,  
1356 Sloane, H.J., 2010. A combined oxygen and silicon diatom isotope  
1357 record of Late Quaternary change in Lake El'gygytyn, North East  
1358 Siberia. *Quat. Sci. Rev.* 29, 774–786.  
1359 <https://doi.org/10.1016/j.quascirev.2009.11.024>
- 1360 Swann, G.E.A., Leng, M.J., Sloane, H.J., Maslin, M.A., Onodera, J., 2007.  
1361 Diatom oxygen isotopes: Evidence of a species effect in the sediment  
1362 record. *Geochemistry, Geophys. Geosystems* 8, Q06012.  
1363 <https://doi.org/10.1029/2006GC001535>
- 1364 Swann, G.E.A., Mackay, A.W., Vologina, E., Jones, M.D., Panizzo, V.N.,  
1365 Leng, M.J., Sloane, H.J., Snelling, A.M., Sturm, M., 2018. Lake Baikal  
1366 isotope records of Holocene Central Asian precipitation. *Quat. Sci. Rev.*  
1367 189, 210–222. <https://doi.org/10.1016/J.QUASCIREV.2018.04.013>
- 1368 Swann, G.E.A., Patwardhan, S. V, 2011. Application of Fourier Transform  
1369 Infrared Spectroscopy (FTIR) for assessing biogenic silica sample purity  
1370 in geochemical analyses and palaeoenvironmental research. *Clim. Past*  
1371 7, 65–74. <https://doi.org/10.5194/cp-7-65-2011>
- 1372 Tarasov, P., Bezrukova, E., Karabanov, E., Nakagawa, T., Wagner, M.,  
1373 Kulagina, N., Letunova, P., Abzaeva, A., Granoszewski, W., Riedel, F.,  
1374 2007. Vegetation and climate dynamics during the Holocene and  
1375 Eemian interglacials derived from Lake Baikal pollen records.  
1376 *Palaeogeogr. Palaeoclimatol. Palaeoecol.* 252, 440–457.  
1377 <https://doi.org/10.1016/J.PALAEO.2007.05.002>
- 1378 Tarasov, P.E., Bezrukova, E. V., Krivonogov, S.K., 2009. Late Glacial and  
1379 Holocene changes in vegetation cover and climate in southern Siberia  
1380 derived from a 15 kyr long pollen record from Lake Kotokel. *Clim. Past*  
1381 Discuss. 5, 127–151. <https://doi.org/10.5194/cpd-5-127-2009>
- 1382 Tchebakova, N.M., Parfenova, E., Soja, A.J., 2009. The effects of climate,  
1383 permafrost and fire on vegetation change in Siberia in a changing  
1384 climate. *Environ. Res. Lett.* 4, 045013. <https://doi.org/10.1088/1748-9326/4/4/045013>
- 1386 Tchebakova, N.M., Parfenova, E.I., Soja, A.J., 2011. Climate change and  
1387 climate-induced hot spots in forest shifts in central Siberia from  
1388 observed data. *Reg. Environ. Chang.* 11, 817–827.  
1389 <https://doi.org/10.1007/s10113-011-0210-4>
- 1390 Teller, J.T., Leverington, D.W., Mann, J.D., 2002. Freshwater outbursts to

- 1391 the oceans from glacial Lake Agassiz and their role in climate change  
 1392 during the last deglaciation. *Quat. Sci. Rev.* 21, 879–887.  
 1393 [https://doi.org/10.1016/S0277-3791\(01\)00145-7](https://doi.org/10.1016/S0277-3791(01)00145-7)
- 1394 Terzer, S., Wassenaar, L.I., Araguás-Araguás, L.J., Aggarwal, P.K., 2013.  
 1395 Global isoscapes for delta18O and delta2H in precipitation: improved  
 1396 prediction using regionalized climatic regression models. *Hydrol. Earth*  
 1397 *Syst. Sci. Discuss.* 10, 7351–7393. [https://doi.org/10.5194/hessd-10-](https://doi.org/10.5194/hessd-10-7351-2013)  
 1398 [7351-2013](https://doi.org/10.5194/hessd-10-7351-2013)
- 1399 Tingley, M.P., Huybers, P., 2013. Recent temperature extremes at high  
 1400 northern latitudes unprecedented in the past 600 years. *Nature* 496,  
 1401 201–205. <https://doi.org/10.1038/nature11969>
- 1402 Tsygankov, A.A., Matukov, D.I., Berezhnaya, N.G., Larionov, A.N.,  
 1403 Posokhov, V.F., Tsyrenov, B.T., Khromov, A.A., Sergeev, S.A., 2007.  
 1404 Late Paleozoic granitoids of western Transbaikalia: magma sources and  
 1405 stages of formation. *Russ. Geol. Geophys.* 48, 120–140.  
 1406 <https://doi.org/10.1016/J.RGG.2006.12.011>
- 1407 Tubi, A., Dayan, U., 2013. The Siberian High: teleconnections, extremes and  
 1408 association with the Icelandic Low. *Int. J. Climatol.* 33, 1357–1366.  
 1409 <https://doi.org/10.1002/joc.3517>
- 1410 Tzedakis, P.C., Crucifix, M., Mitsui, T., Wolff, E.W., 2017. A simple rule to  
 1411 determine which insolation cycles lead to interglacials. *Nature* 542, 427–  
 1412 432. <https://doi.org/10.1038/nature21364>
- 1413 Ufimtsev, G.F., Shchetnikov, A.A., Filinov, I.A., 2009. Neotectonic inversions  
 1414 in the Baikal Rift System. *Russ. Geol. Geophys.* 50, 618–627.  
 1415 <https://doi.org/10.1016/j.rgg.2008.12.006>
- 1416 van Hardenbroek, M., Chakraborty, A., Davies, K.L., Harding, P., Heiri, O.,  
 1417 Henderson, A.C.G., Holmes, J.A., Lasher, G.E., Leng, M.J., Panizzo,  
 1418 V.N., Roberts, L., Schilder, J., Trueman, C.N., Wooller, M.J., 2018. The  
 1419 stable isotope composition of organic and inorganic fossils in lake  
 1420 sediment records: Current understanding, challenges, and future  
 1421 directions. *Quat. Sci. Rev.* 196, 154–176.  
 1422 <https://doi.org/10.1016/J.QUASCIREV.2018.08.003>
- 1423 Wang, Y.J., Cheng, H., Edwards, R.L., An, Z.S., Wu, J.Y., Shen, C.C.,  
 1424 Dorale, J.A., 2001. A high-resolution absolute-dated late Pleistocene  
 1425 Monsoon record from Hulu Cave, China. *Science* 294, 2345–2348.  
 1426 <https://doi.org/10.1126/science.1064618>
- 1427 Wanner, H., Solomina, O., Grosjean, M., Ritz, S.P., Jetel, M., 2011. Structure  
 1428 and origin of Holocene cold events. *Quat. Sci. Rev.* 30, 3109–3123.  
 1429 <https://doi.org/10.1016/j.quascirev.2011.07.010>
- 1430 Weninger, B., Jöris, O., 2008. A 14C age calibration curve for the last 60 ka:  
 1431 the Greenland-Hulu U/Th timescale and its impact on understanding the  
 1432 Middle to Upper Paleolithic transition in Western Eurasia. *J. Hum. Evol.*  
 1433 55, 772–781. <https://doi.org/10.1016/j.jhevol.2008.08.017>



- 1434 Williams, D.F., Peck, J., Karabanov, E.B., Prokopenko, A.A., Kravchinsky,  
1435 V., King, J., Kuzmin, M.I., 1997. Lake Baikal Record of Continental  
1436 Climate Response to Orbital Insolation During the Past 5 Million Years.  
1437 *Science* 278, 1114–1117.  
1438 <https://doi.org/10.1126/science.278.5340.1114>
- 1439 Williams, J.W., Blois, J.L., Shuman, B.N., 2011. Extrinsic and intrinsic forcing  
1440 of abrupt ecological change: case studies from the late Quaternary. *J.*  
1441 *Ecol.* 99, 664–677. <https://doi.org/10.1111/j.1365-2745.2011.01810.x>
- 1442 Wilson, K.E., Leng, M.J., Mackay, A.W., 2014. The use of multivariate  
1443 statistics to resolve multiple contamination signals in the oxygen isotope  
1444 analysis of biogenic silica. *J. Quat. Sci.* 29, 641–649.  
1445 <https://doi.org/10.1002/jqs.2729>
- 1446 Yakhnenko, V.M., Mamontov, A.M., Luczynski, M., 2008. East-Siberian  
1447 coregonid fishes: their occurrence, evolution and present status.  
1448 *Environ. Biotechnol.* 4, 41–53.
- 1449 Zhang, W., Yan, H., Dodson, J., Cheng, P., Liu, C., Li, J., Lu, F., Zhou, W.,  
1450 An, Z., 2018. The 9.2 ka event in Asian summer monsoon area: the  
1451 strongest millennial scale collapse of the monsoon during the Holocene.  
1452 *Clim. Dyn.* 50, 2767–2782. <https://doi.org/10.1007/s00382-017-3770-2>
- 1453